

# Partially gapped fermions in 2D

Jonas de Woul and Edwin Langmann

*Theoretical Physics, KTH*  
*SE-10691 Stockholm, Sweden*  
 jodw02@kth.se and langmann@kth.se

## Abstract

We compute mean field phase diagrams of two closely related interacting fermion models in two spatial dimensions (2D). The first is the so-called 2D  $t$ - $t'$ - $V$  model describing spinless fermions on a square lattice with local hopping and density-density interactions. The second is the so-called 2D Luttinger model that provides an effective description of the 2D  $t$ - $t'$ - $V$  model and in which parts of the fermion degrees of freedom are treated exactly by bosonization. In mean field theory, both models have a charge-density-wave (CDW) instability making them gapped at half-filling. The 2D  $t$ - $t'$ - $V$  model has a significant parameter regime away from half-filling where neither the CDW nor the normal state are thermodynamically stable. We show that the 2D Luttinger model allows to obtain more detailed information about this mixed region. In particular, we find in the 2D Luttinger model a partially gapped phase that, as we argue, can be described by an exactly solvable model.

## 1 Introduction

This is the second in a series of papers that aim to develop a method to do reliable computations in a spinless 2D lattice fermion model of Hubbard type; see [1] for a concise summary. In the first paper in this series [2], an effective model for the low-energy physics of the lattice system was derived. It was shown that parts of the fermion degrees of freedom in the model can be treated exactly using bosonization. In this paper, we apply mean field methods to the remaining degrees of freedom. We present analytical and numerical results showing that our method is useful for obtaining quantitative physical information about the lattice fermions.

### 1.1 Motivation

The difficulty to do reliable computations in 2D lattice fermion models of Hubbard-type has remained an outstanding challenge in theoretical physics for many years. One can hope

that a solution to this problem will be a key step towards a satisfactory theory of high-temperature superconductors [3]. One simple example is the so-called 2D  $t$ - $t'$ - $V$  model describing spinless fermions on a square lattice with local hopping and density-density interactions; see Section 2.1 for a precise definition. One of us (EL) proposed a particular partial continuum limit of this lattice system [1, 2]. This leads to an interacting model of so-called nodal fermions, which have linear band relations, coupled to so-called antinodal fermions with hyperbolic band relations. It was found that this is a natural 2D analogue of the Luttinger model, not only in that it arises as a continuum limit of the 2D  $t$ - $t'$ - $V$  model, but also since the nodal fermions can be bosonized and thus treated exactly. In particular, it is possible to integrate out the bosonized nodal fermions and thus obtain an effective model for the antinodal fermions; see Section 2.2.

In this paper we use mean field theory to address the question if and when the antinodal fermions in this 2D Luttinger model have a gap. These are key questions since if the antinodal fermions are gapped they do not contribute to the low-energy physics. We then obtain an effective Hamiltonian of nodal fermions that is exactly solvable. We find a significant parameter regime away from half-filling where this is indeed the case. As a motivation for our work, we also present mean fields results for the 2D  $t$ - $t'$ - $V$  model that show that there is an interesting region away from half filling where a direct application of mean field theory fails. We find that this regime becomes accessible to mean field theory by using the 2D Luttinger model.

We recall the key parameters of these two models. The 2D  $t$ - $t'$ - $V$  model is characterized by the nearest-neighbor (nn) hopping constant  $t > 0$ , the next-nn (nnn) hopping constant  $-t/2 < t' < t/2$ , the nn density-density coupling strength  $V/2 > 0$ , and the filling factor  $0 \leq \nu \leq 1$  (see Section 2.1 for more details). The 2D Luttinger model depends on two additional parameters,  $\kappa$  and  $Q$ , which have the following significance. To derive the model, it is assumed that there is an underlying Fermi surface that, when the system is near half-filling, is a line segment in each nodal region. These are the so called nodal Fermi surface arcs, and the parameter  $0 \leq \kappa \leq 1$  determines the size of these arcs. Furthermore, the parameter  $Q \approx \pi/2$  fixes the point about which the nodal band relations are linearized; the details are given in Section 2.2. One important question addressed in this paper is how to fix the parameter  $Q$ .

## 1.2 Mean field phase diagrams

Two-dimensional lattice fermion systems with repulsive interactions are often insulators at half-filling, but away from half-filling there are competing tendencies that lead to rich Hartree-Fock (HF) phase diagrams. A well-known example is the 2D Hubbard model which, at half-filling, has an insulating antiferromagnetic (AF) HF ground state [4]. However, away from half-filling, unrestricted HF theory yields intricate solutions that include domain walls, vortices, polarons etc. imposed on an AF background; see e.g. [5] and references therein. These solutions suggest that the pure AF state is only stable at half-filling and that additional holes or particles tend to distribute so as to perturb the AF state as little as possible. Furthermore, away from half-filling, these solutions break translational invariance in a complicated manner and are highly degenerate. One thus expects that the low-energy

properties of the lattice model away from half-filling should be dominated by fluctuations between these degenerate solutions. Unfortunately, it is difficult to formulate a useful low-energy effective model for this situation.

Unrestricted HF theory is computationally demanding and thus applicable only for moderate lattice sizes. However, it is possible to find “mixed” regions in the phase diagram, i.e. regions with intricate and highly degenerate HF solutions, already in mean field theory. By the latter we mean HF theory restricted to states invariant under translations by two sites [6, 7]. This requires little computational effort and thus allows to explore the full phase diagram for arbitrarily large lattice sizes. In this manner one can identify the regions in the phase diagram in which an exotic physical behavior can be expected. It is remarkable how rich the resulting mean field diagrams for the 2D Hubbard model are [7].

In this paper we present mean field phase diagrams for the 2D  $t$ - $t'$ - $V$  model, which is a spinless variant of the Hubbard model and therefore somewhat simpler. We find a stable charge-density-wave (CDW) mean field ground state at half-filling  $\nu = 0.5$ , a translation-invariant normal (N) state far away from half-filling, and extended doping regions with mixed phases in-between. We indicate the mixed phases in our phase diagrams by horizontal lines to emphasize that mean field theory fails here, i.e. it does not allow any specific conclusions to be drawn; see Figure 1(a). Put differently, the mixed regions are “unknown territories” (analogous to white spots on ancient maps) for mean field theory, but the knowledge of their existence is nevertheless important physical information.

Our main result is to show that the 2D Luttinger model provides a tool to explore these “unknown territories” using mean field theory for the antinodal fermions. To be more specific, we compute mean field phase diagrams for the effective antinodal Hamiltonian defined in Section 2.2. We find that the antinodal fermions indeed have a CDW gap in a significant region of the parameter space, as conjectured in [1, 2]. We refer to this also as a CDW phase, but we emphasize that, in general, it corresponds to a *partially gapped phase* of the 2D Luttinger model. There are also the nodal fermions that are gapless, and these fermions can dope the system even if the antinodal fermions remain gapped and half-filled. In this way a large part of the mixed regions of the phase diagram for the 2D  $t$ - $t'$ - $V$  model is filled in; see Figure 1(b). We also study how sensitive the occurrence of a partially gapped phase is to variations in the model parameters, especially  $\kappa$  and  $Q$ .

### 1.3 Related work

The derivation of the 2D Luttinger model was inspired by important work of Mattis [8], Schulz [9], Luther [10], and Furukawa *et al.* [11]; see [2] for discussion and further references.

The phase diagram of the 2D  $t$ - $t'$ - $V$  model, at and away from half-filling, has been studied using various techniques. Recent work close to ours is [12] in which the possibility of phase separation is investigated; see also [13, 14]. In particular, Figure 1(a) in [12] is the same as our Figure 1(a). Note though, unlike [12], we do not necessarily interpret the horizontally lined region in our Figure 1(a) as a phase-separated state. Instead, we only conclude that the considered mean field theory fails to give a stable homogeneous phase

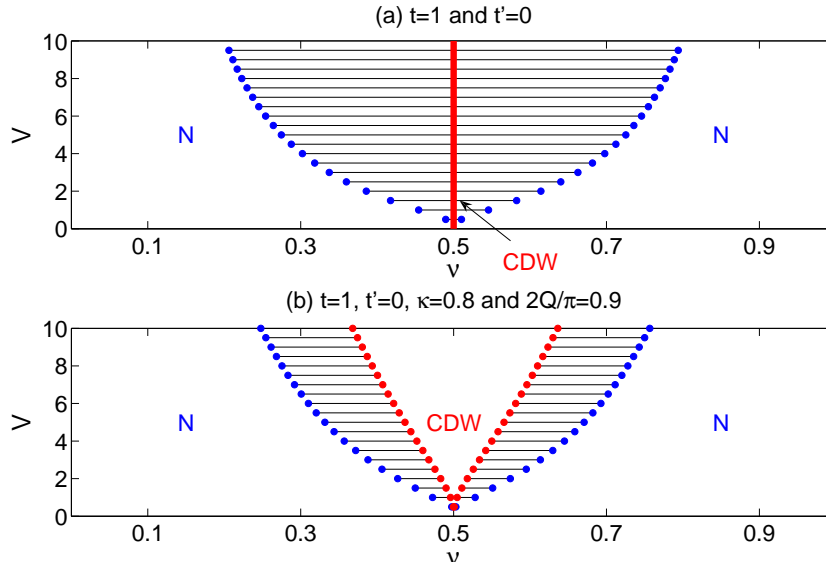


Figure 1: Comparison between the coupling ( $V$ ) vs. filling ( $\nu$ ) mean field phase diagrams of the 2D  $t$ - $t'$ - $V$  model (a) and the 2D Luttinger model (b) for  $t = 1$  and  $t' = 0$ . Shown are the charge-density-wave (CDW) and normal (N) phases as a function of coupling and filling at zero temperature. The regimes marked by horizontal lines are mixed, i.e. neither the CDW nor the N phase is thermodynamically stable. The CDW phase in (a) exists only at half-filling  $\nu = 0.5$ . The CDW phase in (b) corresponds to a partially gapped phase.

there.

One motivation for our work are experimental results on high temperature superconductors. It is known from angle-resolved photoemission spectroscopy [15] that these materials can have an electronic phase in which parts of the underlying Fermi surface do not have gapless excitations. In particular, for hole-doped materials, one finds near half-filling that the degrees of freedom in the antinodal regions are gapped, while in each nodal region there is an ungapped Fermi surface arc; see e.g. Figure 5 in [16] or Figure 1 in [17].<sup>1</sup> We believe that this suppression of accessible electronic states at the Fermi level seen in experiments provide strong support for our approach. However, we stress that the emphasis of the present work is mathematical, and a confrontation of our results with experiments is postponed to future work.

---

<sup>1</sup>The experimental situation for electron-doped materials is different and its relation to the present work will not be discussed here.

## 1.4 Notation and conventions

We use the symbol “ $\stackrel{\text{def}}{=}$ ” to emphasize that an equation is a definition. We denote by  $\text{Re}(c)$  and  $\text{Im}(c)$  the real- and imaginary parts of a complex number  $c$ , and  $\bar{c}$  is its complex conjugate. We write “ $a_{0,1} = A \pm B$ ” short for “ $a_0 = A + B$  and  $a_1 = A - B$ ” etc. We use bold symbols for matrices, e.g.  $\mathbf{1}$  is the identity matrix. By “ $X = 2.31(1)$ ” we mean a numerical result “ $X = 2.31 \pm 0.01$ ”.

The fermion models considered in this paper are defined by Hamiltonians of the following generic type

$$H = \sum_{kl} (t_{kl} - \mu \delta_{kl}) c_k^\dagger c_l + \sum_{klmn} v_{klmn} c_k^\dagger c_l^\dagger c_n c_m \quad (1)$$

with fermion operators  $c_k^{(\dagger)}$  labeled by a finite number  $\mathcal{N}$  of one-particle quantum numbers  $k$ . Note that  $\mathcal{N}$  equals the number of one-particle degrees of freedom that are included in the model. Our normalization is such that

$$\{c_j, c_k^\dagger\} = \delta_{jk}. \quad (2)$$

The model parameters  $t_{kl} = \overline{t_{lk}}$  and  $v_{klmn} = \overline{v_{mnlk}}$  correspond to the matrix elements of the kinetic energy and two-body interaction potential, respectively, and  $\mu$  is the chemical potential. The model is defined on a fermion Fock space with a vacuum  $|0\rangle$  annihilated by all  $c_k$ . Expectation values with respect to a given state of the model (both zero and non-zero temperatures) are denoted by  $\langle \cdot \rangle$ . The state can be either the exact thermal equilibrium state or an approximate Hartree-Fock state; it will always be clear from the context which is meant. The inverse temperature is denoted by  $\beta > 0$ .

## 1.5 Plan of paper

The two models we consider are defined in Section 2. Some results presented here are (minor) generalizations of the corresponding ones in [2], as further elaborated in Appendix A. Section 3 explains the method we use to compute mean field phase diagrams, with some technical details deferred to appendices B and C. Our results are given and discussed in Section 4. Section 5 gives some closing remarks.

## 2 Models

In this section, we define the two studied models and discuss the relation between them. We note in passing that the notation used here is slightly different from that in [2]; see Appendix A.1 for details.

## 2.1 2D $t$ - $t'$ - $V$ model

The 2D  $t$ - $t'$ - $V$  model describes spinless fermions on a square lattice with  $L^2$  sites and lattice constant  $a = 1$ . The fermions hop with amplitudes  $t$  and  $t'$  between nn and nnn sites, and fermions on nn sites interact with a density-density interaction of strength  $V/2$ . The Hamiltonian is given in Fourier space by

$$H_{tt'V} = \sum_{\mathbf{k} \in \text{BZ}} [\epsilon(\mathbf{k}) - \mu] c^\dagger(\mathbf{k}) c(\mathbf{k}) + \frac{V}{2L^2} \sum_{\mathbf{k}_j \in \text{BZ}} v_{\mathbf{k}_1, \mathbf{k}_2, \mathbf{k}_3, \mathbf{k}_4} c^\dagger(\mathbf{k}_1) c^\dagger(\mathbf{k}_3) c(\mathbf{k}_4) c(\mathbf{k}_2) \quad (3)$$

with the tight-binding band relation ( $\mathbf{k} = (k_1, k_2)$ )

$$\epsilon(\mathbf{k}) = -2t[\cos(k_1) + \cos(k_2)] - 4t' \cos(k_1) \cos(k_2) \quad (4)$$

and the interaction vertex<sup>2</sup>

$$v_{\mathbf{k}_1, \mathbf{k}_2, \mathbf{k}_3, \mathbf{k}_4} = u(\mathbf{k}_1 - \mathbf{k}_2) \sum_{\mathbf{n} \in \mathbb{Z}^2} \delta_{\mathbf{k}_1 - \mathbf{k}_2 + \mathbf{k}_3 - \mathbf{k}_4, 2\pi \mathbf{n}} \quad (5)$$

with

$$u(\mathbf{p}) = \cos(p_1) + \cos(p_2). \quad (6)$$

The fermion operators  $c^{(\dagger)}(\mathbf{k})$  are labeled by momenta  $\mathbf{k}$  in the Brillouin zone

$$\text{BZ} \stackrel{\text{def}}{=} \left\{ \mathbf{k} = (k_1, k_2) \mid -\pi < k_j < \pi, k_j = \frac{2\pi}{L}(n_j + \frac{1}{2}), n_j \in \mathbb{Z}, j = 1, 2 \right\}. \quad (7)$$

Other conventions used are explained in Section 1.4 (with the  $k$  there corresponding to our  $\mathbf{k}$  here). Note that the number of different one-particle quantum numbers  $\mathbf{k}$  equals the system volume,  $\mathcal{N} = L^2$ . The chemical potential  $\mu$  is to be determined such that the fermion density

$$\nu \stackrel{\text{def}}{=} \frac{1}{L^2} \langle N \rangle, \quad N \stackrel{\text{def}}{=} \sum_{\mathbf{k} \in \text{BZ}} c^\dagger(\mathbf{k}) c(\mathbf{k}) \quad (8)$$

has a fixed specified value. We refer to  $\nu$  as *filling factor* or filling, and  $\nu - 0.5$  is called *doping*. The filling lies in the range  $0 \leq \nu \leq 1$ , and  $\nu = 0.5$  corresponds to half-filling. We always assume  $-t/2 < t' < t/2$ ,  $V > 0$ , and that  $L/2$  is an integer. To simplify notation we set  $t = 1$  in all figures, i.e. energies are measured in units of  $t$ . Figure 2 shows the Brillouin zone of this model and a typical example of a non-interacting Fermi surface defined by  $\epsilon(\mathbf{k}) = \mu$ .

Note that we use anti-periodic boundary conditions and a large-distance cutoff different to that used when deriving the 2D Luttinger model in [2]. This is legitimate since we are interested in the thermodynamic limit  $L \rightarrow \infty$ , and finite size effects are negligible for the system sizes ( $L \geq 100$ ) we use in our numerical computations.

The invariance of the 2D  $t$ - $t'$ - $V$  model under particle-hole transformations provides an important guide for us. The interested reader can find more details in Appendix A.1.

---

<sup>2</sup>The sum over  $\mathbf{n}$  in (5) takes into account possible umklapp processes.

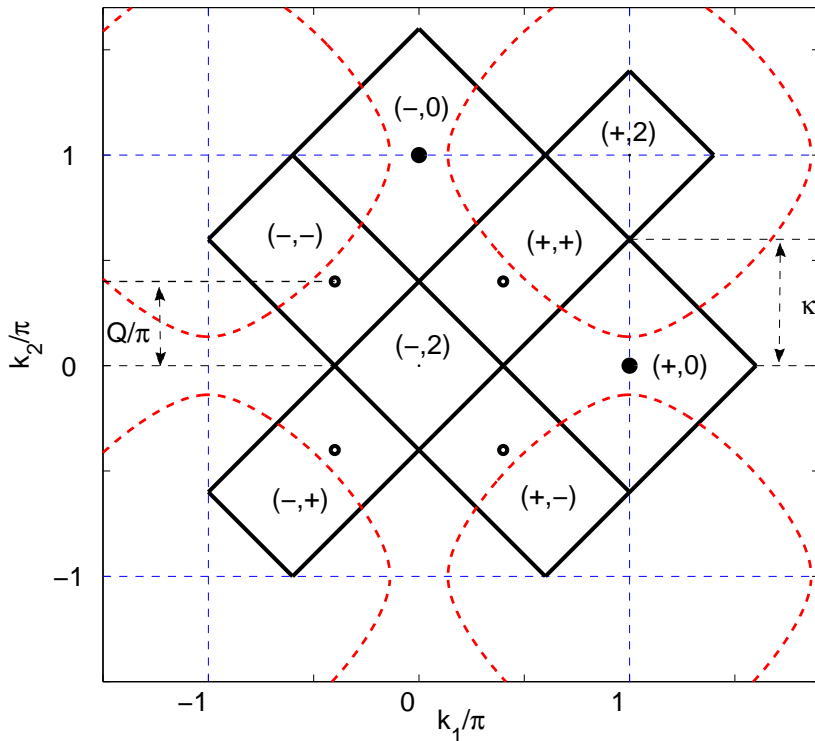


Figure 2: Fermi surface for the tight-binding band relation in (4) with  $t = 1$ ,  $t' = -0.2$  and  $\mu = -0.51(1)$  (bent dashed curves). Also indicated are the eight regions labeled by  $(r, s)$  and discussed in the main text (large squares for  $r = \pm$ ,  $s = 0$ , rectangles for  $r = \pm$ ,  $s = \pm$ , and small squares for  $r = \pm$ ,  $s = 2$ ). Note that the Brillouin zone is equal to the union of these regions. The two antinodal points  $\mathbf{Q}_{r,0}$  and four nodal points  $\mathbf{Q}_{r,\pm}$  are depicted by dots and rings, respectively. The parameters used in the plot are  $\kappa = 0.6$  and  $Q/\pi = 0.4$ , and  $\mu$  corresponds to  $Q_0/\pi = 0.45(1)$ .

## 2.2 2D Luttinger model

A detailed derivation of the 2D Luttinger model and its partial solution by bosonization were given in [2]. Here we first describe this model and then summarize the results from [2] that we actually need.

The 2D Luttinger model involves six fermion flavors labeled by a pair of indices  $(r, s)$  with  $r = \pm$  and  $s = 0, \pm$ . These flavors correspond to different regions in the Brillouin zone of the 2D  $t$ - $t'$ - $V$  model, as shown in Figure 2 (two large squares for  $s = 0$  and four large

rectangles for  $s = \pm$ ). The sizes of these regions are determined by a parameter  $\kappa$  in the range  $0 \leq \kappa \leq 1$  (we used  $\kappa = 0.6$  in Figure 2). There are two more fermion flavors with  $r = \pm$  and  $s = 2$  (two small squares in Figure 2), but in this paper we assume that the parameters are such that the  $s = 2$  fermions are far away in energy from the Fermi level and thus their dynamics can be ignored [2] (we discuss this point in Section 5, Remark 2).

The momenta in the regions with  $s = 0$  can be written as  $\mathbf{Q}_{\pm,0} + \mathbf{k}$  with

$$\mathbf{Q}_{+,0} = (\pi, 0), \quad \mathbf{Q}_{-,0} = (0, \pi) \quad (9)$$

and  $\mathbf{k}$  in

$$\Lambda_a^* \stackrel{\text{def}}{=} \left\{ \mathbf{k} \in \text{BZ} \mid |k_1 \pm k_2| \leq \kappa\pi, \quad k_1 \pm k_2 = \frac{2\sqrt{2}\pi}{L}(n_{\pm} + \frac{1}{2}), \quad n_{\pm} \in \mathbb{Z} \right\}. \quad (10)$$

Close to the points  $\mathbf{Q}_{r,0}$ ,  $r = \pm$ , the band relation in (4) can be well approximated by the lowest-order non-trivial terms in a Taylor series expansion  $\epsilon(\mathbf{Q}_{r,0} + \mathbf{k}) \approx 4t' + \epsilon_r(\mathbf{k})$  with

$$\epsilon_r(\mathbf{k}) = rt(k_1^2 - k_2^2) - 2t'(k_1^2 + k_2^2), \quad (11)$$

i.e.  $\mathbf{Q}_{r,0}$  correspond to saddle points of  $\epsilon(\mathbf{k})$  if  $-t/2 < t' < t/2$ . This also explains why we impose these bounds on  $t'$ . Similarly, the band relation for fermion degrees of the freedom corresponding to  $s = \pm$  can be well approximated by bands linear in  $(k_1 \pm k_2)$  close to the points  $\mathbf{Q}_{r,\pm} = (rQ, \pm rQ)$  with  $Q$  another free parameter ( $r = +$  or  $-$ ). We use standard terminology [15] and refer to the fermions with  $s = 0$  as *antinodal* and the fermions with  $s = \pm$  as *nodal*, respectively. In Figure 2 the antinodal points  $\mathbf{Q}_{r,0}$  are indicated by dots and the nodal points  $\mathbf{Q}_{r,\pm}$  by circles.

The 2D Luttinger model is defined by a Hamiltonian of the form  $H_n + H_a + H_{na}$  where  $H_n$  and  $H_a$  include terms depending only on the nodal and antinodal fermions, respectively, and  $H_{na}$  are interaction terms with both kinds of fermions. It is obtained from the 2D  $t$ - $t'$ - $V$  model by certain approximations that amount to a particular partial continuum limit [2]. A key assumption is that there is an underlying Fermi surface in the nodal regions  $s = \pm$  consisting of line segments (“Fermi surface arcs”) and containing the nodal points  $(rQ_0, \pm rQ_0)$  for some  $Q_0 \approx \pi/2$  determined by  $\mu$ ,  $\kappa$  and  $Q$ ; see (49). In [2] we fixed  $\mu$  by the condition  $Q_0 = Q$ , but in the present paper we work in the grand canonical ensemble and thus allow  $\mu$  (i.e.  $Q_0$ ) to be arbitrary in intermediate steps of our computations. No assumption is made on the Fermi surface in the antinodal regions.

As explained in [2], Sections 2 and 6.2, we need to restrict ourselves to parameters such that

$$(1 - \kappa)\pi/2 < Q < (1 + \kappa)\pi/2 \quad \text{and} \quad 0 \leq \frac{V(1 - \kappa)\sin(Q)}{2\pi[t + 2t'\cos(Q)]} < 1 \quad (12)$$

with the same bound for  $Q_0$  as for  $Q$ . Moreover, we require  $Q_0$  and  $Q$  to be different from  $\pi/2$ , since otherwise one has additional back-scattering terms in the 2D Luttinger model which spoil a simple treatment of the nodal fermions using bosonization; see [2]. These conditions define the parameter regime of interest to us.

The nodal fermions in the 2D Luttinger model can be bosonized and integrated out exactly. This yields an effective model for the antinodal fermions  $c_{\pm}^{(\dagger)}(\mathbf{k}) \stackrel{\text{def}}{=} c^{(\dagger)}(\mathbf{Q}_{\pm,0} + \mathbf{k})$



that, in the local-time approximation [2], is given by a Hamiltonian of the form

$$\tilde{H}_a = \sum_{\mathbf{k} \in \Lambda_a^*} \sum_{r=\pm} [\varepsilon_r(\mathbf{k}) - \mu_a] c_r^\dagger(\mathbf{k}) c_r(\mathbf{k}) + \frac{2g_a}{L^2} \sum_{\mathbf{k}_j \in \Lambda_a^*} \delta_{\mathbf{k}_1 - \mathbf{k}_2 + \mathbf{k}_3 - \mathbf{k}_4, 0} c_+^\dagger(\mathbf{k}_1) c_-^\dagger(\mathbf{k}_3) c_-(\mathbf{k}_4) c_+(\mathbf{k}_2). \quad (13)$$

This Hamiltonian is also of the generic type discussed in Section 1.4 (with the one-particle quantum numbers  $k$  used there to be identified with  $(r, \mathbf{k})$  here). Note that there are  $(\kappa L)^2/2$  different momenta  $\mathbf{k}$ , and that the number of one-particle degrees of freedom in the model is  $\mathcal{N} = (\kappa L)^2$ . The filling factor of the antinodal fermions is therefore

$$\nu_a \stackrel{\text{def}}{=} \frac{1}{(\kappa L)^2} \langle N_a \rangle, \quad N_a \stackrel{\text{def}}{=} \sum_{\mathbf{k} \in \Lambda_a^*} \sum_{r=\pm} c_r^\dagger(\mathbf{k}) c_r(\mathbf{k}), \quad (14)$$

while the total filling factor of the 2D Luttinger model is (including the nodal fermions etc.)

$$\nu = \frac{1}{2} + (1 - \kappa) \left( \frac{2Q_0}{\pi} - 1 \right) + \kappa^2 \left( \nu_a - \frac{1}{2} \right); \quad (15)$$

see [2]. It is  $\nu$  in (15) that is to be identified with the filling factor of the 2D  $t$ - $t'$ - $V$  model.

A main result in [2] are explicit formulas for the parameters  $\mu_a$  and  $g_a$  in terms of the other model parameters:

$$\mu_a = \mu - 2V\nu - 4t' + g_a \nu_a \kappa^2 \quad (16)$$

and

$$g_a = 2V - g_{\text{eff}} \quad (17)$$

with

$$g_{\text{eff}} = \frac{V^2(1 - \kappa)}{\sin(Q)\pi[t + 2t' \cos(Q) + \frac{V}{\pi}(1 - \kappa) \sin(Q)]}. \quad (18)$$

The parameter  $Q_0$  can be computed from the following identity

$$\mu = \sqrt{2}v_F(Q_0 - Q) + 2V\nu - 4t \cos(Q) - 4t' \cos^2(Q) - 2VC \cos(Q) \quad (19)$$

with

$$v_F = 2\sqrt{2} \sin(Q)[t + 2t' \cos(Q)] \quad (20)$$

and where we have introduced a convenient short-hand notation

$$C \stackrel{\text{def}}{=} (1 - \kappa) \cos(Q) \left( \frac{2Q_0}{\pi} - 1 \right) + \frac{1}{2}(1 - \kappa)^2. \quad (21)$$

The constant  $-g_{\text{eff}}$  corresponds to a renormalization of the bare antinodal interaction  $2V$  and arises from integrating out the bosonized nodal fermions.

The 2D  $t$ - $t'$ - $V$  Hamiltonian is equivalent (in a low-energy approximation) to the effective antinodal Hamiltonian in (13) only if one takes into account the additive constant (see Appendix A.2)

$$\mathcal{E}_a = \mathcal{E}_{kin} + \mathcal{E}_u + \mathcal{E}_{int} + \mathcal{E}_n \quad (22)$$

with

$$\begin{aligned} \mathcal{E}_{kin}/L^2 = & \frac{1}{2}(1 - \kappa)^2(-4(t + t') + \frac{1}{3}(t + 2t')(1 - \kappa)^2\pi^2) + (1 - \kappa)(\frac{2Q_0}{\pi} - 1 + \kappa) \\ & \times (\sqrt{2}v_F(Q_0/2 - Q + \pi(1 - \kappa)/4) - 4t \cos(Q) - 4t' \cos^2(Q)), \end{aligned} \quad (23)$$

$$\mathcal{E}_u/L^2 = (\mu - 2V\nu)\nu_a\kappa^2 + \frac{1}{2}g_a\nu_a^2\kappa^4, \quad (24)$$

and

$$\mathcal{E}_{int}/L^2 = -\mu\nu + V\nu^2 + V[\kappa(1 - \kappa) \cos(Q)]^2 - VC^2. \quad (25)$$

The constant  $\mathcal{E}_n$  is derived in [2], but in the present paper we only need that it is independent of the chemical potential:

$$\frac{\partial(\mathcal{E}_n/L^2)}{\partial\mu} = 0. \quad (26)$$

As we show later, the parameter  $Q$  can be fixed by the self-consistency condition  $Q = Q_0$ . Thus the effective antinodal model contains one more free parameter as compared to the 2D  $t$ - $t'$ - $V$  model, namely  $\kappa$ .

As already mentioned, the results in [2] are restricted to the special case in which  $\mu$  is explicitly fixed by the condition  $Q_0 = Q$ , and they are written in a slightly different form. The interested reader can find details about how to obtain the results given here from the ones in [2] in Appendix A.2.

It is not essential to work with the Taylor expansion of the antinodal band relations, and one can equally well use the full band relations

$$\varepsilon_r^{(0)}(\mathbf{k}) = \varepsilon(\mathbf{Q}_{r,0} + \mathbf{k}) - \varepsilon(\mathbf{Q}_{r,0}) \quad (27)$$

instead of (11). As we will discuss, the results for the band relations in (11) and (27) agree quite well for smaller values of  $\kappa$ , but for  $\kappa$  close to one there are some quantitative differences. Furthermore, in the derivation of the 2D Luttinger model, certain approximations were done on the interaction vertex of the 2D  $t$ - $t'$ - $V$  model; see Section 5 in [2]. It was argued that this had no important consequences for low-energy scattering processes. We note here that these approximations were only necessary for processes that include nodal fermions, and it would be possible to use the full interaction vertex for processes involving just antinodal fermions. With this, and using the full band relation (27), one could derive a refined 2D Luttinger model for which the 2D  $t$ - $t'$ - $V$  model is recovered by setting  $\kappa = 1$ .

We finally mention that the local-time approximation in [2] was only done for simplicity, and it is possible to generalize our treatment here to take into account the full time dependent interaction. We hope to come back to this in the future.

### 3 Method

In this section, we discuss the mean field Hamiltonians used for deriving phase diagrams and the procedure that allows us to identify the mixed regions. More explicit details can be found in appendices B and C.

The fermion models considered in the previous section are defined by Hamiltonians of the type (1). Conventional HF theory at zero temperature and fixed particle number  $N_0$  for such models amounts to considering the set of all variational states of the form  $\eta = c^\dagger(f_1)c^\dagger(f_2)\cdots c^\dagger(f_{N_0})|0\rangle$  with  $c^\dagger(f_j) = \sum_k (f_j)_k c_k^\dagger$  and  $f_j$  orthonormal one-particle states.<sup>3</sup> Using standard terminology, we refer to the states  $\eta$  as Slater determinants. The  $f_j$  are to be chosen so as to minimize the HF energy

$$\Omega_{\text{HF}} \stackrel{\text{def}}{=} \langle \eta, H\eta \rangle. \quad (28)$$

It is straightforward to compute an explicit formula of  $\Omega_{\text{HF}}$  in terms of the one-particle density matrix  $\gamma_{ij} = \sum_{k=1}^{N_0} (f_k)_i \overline{(f_k)_j}$ ; see Appendix B.

In the present paper, we work at (mainly) small but non-zero temperatures (unless otherwise indicated  $\beta = 10^5$ ). This means that we minimize the full grand canonical potential (including the entropy) with respect to all HF Gibbs states; see Appendix B for a full discussion. We will however set the temperature to zero in the current section to not burden the presentation.

### 3.1 2D $t$ - $t'$ - $V$ model

It is convenient to choose the Slater determinant  $\eta$  as ground state of a reference Hamiltonian

$$H_{\text{HF}} = H_0 + \sum_{\mathbf{k}, \mathbf{k}'} w(\mathbf{k}, \mathbf{k}') c^\dagger(\mathbf{k}) c(\mathbf{k}') \stackrel{\text{def}}{=} \sum_{\mathbf{k}, \mathbf{k}'} h_w(\mathbf{k}, \mathbf{k}') c^\dagger(\mathbf{k}) c(\mathbf{k}') \quad (29)$$

with  $H_0$  the non-interacting Hamiltonian obtained from the one in (3) by setting  $V = 0$ , and  $w(\mathbf{k}, \mathbf{k}') = \overline{w(\mathbf{k}', \mathbf{k})}$  the matrix elements of the HF potential  $w$ . This allows to parametrize HF theory by the one-particle Hamiltonian  $h_w$  defined in (29). As explained below, it is important to use the grand canonical ensemble, i.e. to fix the particle number by adjusting the chemical potential  $\mu$  [7]. One thus obtains

$$\gamma(\mathbf{k}, \mathbf{k}') = \sum_k \theta(-e_k) f_k(\mathbf{k}) \overline{f_k(\mathbf{k}')} \quad (30)$$

with  $e_k$  and  $f_k$  the eigenvalues and corresponding orthonormal eigenvectors of  $h_w$  and  $\theta$  the Heaviside function. Note that the chemical potential is included in  $e_k$ .

Unrestricted HF theory amounts to determining the HF potential  $w$  that minimizes  $\Omega_{\text{HF}}$  under the filling constraint

$$\nu = -\frac{\partial(\Omega_{\text{HF}}/L^2)}{\partial\mu}. \quad (31)$$

This method is computationally demanding and thus restricted to small system sizes.

By *mean field theory* we mean the restriction of HF theory to states that are invariant under translations by two sites. As explained in Appendix C.1, this corresponds to considering the following restricted set of HF potentials:

$$w(\mathbf{k}, \mathbf{k}') = (q_0 + q_1[\cos(k_1) + \cos(k_2)]) \delta_{\mathbf{k}, \mathbf{k}'} + \Delta \delta_{\mathbf{k}, \mathbf{k}'+\mathbf{Q}} \quad (32)$$

---

<sup>3</sup>To be more precise: the  $f_j$  are vectors in  $\mathbb{C}^{\mathcal{N}}$  with components  $(f_j)_k$ , and  $\sum_k \overline{(f_i)_k} (f_j)_k = \delta_{ij}$ .

with  $\mathbf{Q} = (\pi, \pi)$  and three real variational parameters  $q_0$ ,  $q_1$  and  $\Delta$ . For  $\Delta = 0$  this corresponds to a normal (N) state that is translation invariant, and for  $\Delta \neq 0$  one has a charge-density-wave (CDW) state for which translation invariance is broken down to translations by two lattice sites. The computational problem is now very easy: there are only three variational parameters, and  $\Omega_{\text{HF}}$  can be computed analytically by Fourier transformation; the interested reader can find details in Appendix C.1.

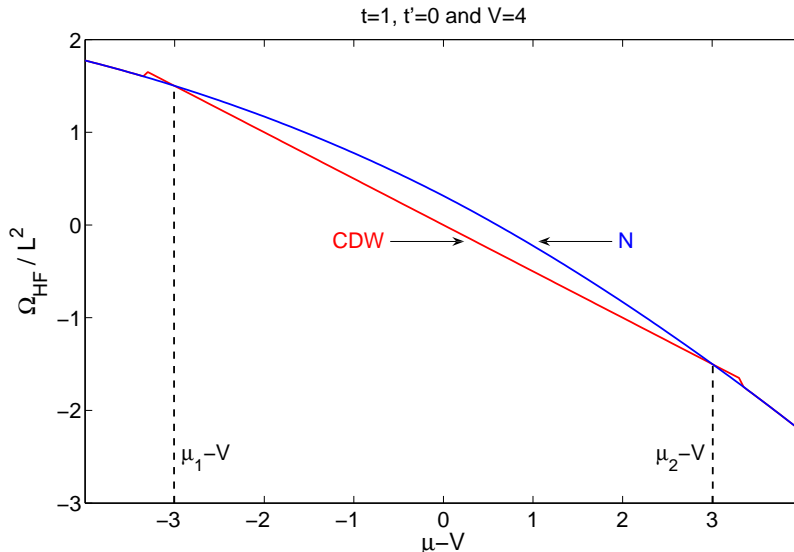


Figure 3: Hartree-Fock energies of the charge-density-wave (CDW) and normal (N) states vs. chemical potential  $\mu$  for the 2D  $t$ - $t'$ - $V$  model at  $t = 1$ ,  $t' = 0$ ,  $V = 4$ . The energy  $\Omega_{\text{HF}}$  of the thermodynamically stable phase is given by the minimum of these curves. The constant slope of the CDW curve in  $\mu_1 < \mu < \mu_2$  implies that the CDW phase can exist only at half-filling, and the kinks at  $\mu = \mu_{1,2}$ , where the system changes from the CDW to the N phase, imply mixed regions where neither the CDW nor the N phase is thermodynamically stable. (A convenient overall constant has been added to  $\Omega_{\text{HF}}$ .)

It is important to note that, by working with the grand canonical ensemble, we not only can detect variational ground states given by Slater determinants  $\eta_{\text{CDW}}$  (with  $\Delta \neq 0$ ) or  $\eta_{\text{N}}$  (with  $\Delta = 0$ ), but it is also possible that the state with lowest energy is mixed and of the form

$$\lambda|\eta_{\text{CDW}}\rangle\langle\eta_{\text{CDW}}| + (1 - \lambda)|\eta_{\text{N}}\rangle\langle\eta_{\text{N}}| \quad (33)$$

for some  $0 < \lambda < 1$ .<sup>4</sup> In general, the two Slater determinants correspond to different filling factors  $\nu_{\text{CDW}}$  and  $\nu_{\text{N}}$ , and the state in (33) corresponds to total filling

$$\nu = \lambda\nu_{\text{CDW}} + (1 - \lambda)\nu_{\text{N}}. \quad (34)$$

The possibility of obtaining (33) can be seen by computing the HF energies for the CDW and N states,  $\Omega_{\text{HF}}^X$  for  $X = \text{CDW}$  and N, as functions of the chemical potential  $\mu$ ; see e.g. Figure 3 for  $t = 1$ ,  $t' = 0$  and  $V = 4$ . One finds two different regimes: there is an interval

<sup>4</sup>We identify a Slater determinant  $\eta$  with the state  $|\eta\rangle\langle\eta|$ .

$\mu_1 < \mu < \mu_2$  where  $\Omega_{\text{HF}}^{\text{CDW}} < \Omega_{\text{HF}}^{\text{N}}$ , i.e. the system clearly has a CDW mean field ground state  $\eta_{\text{CDW}}$ ; for  $V/t = 4$  and  $t' = 0$  we find  $\mu_2 - V = V - \mu_1 = 3.01(1)$ .<sup>5</sup> The second kind of regime is for  $\mu < \mu_1$  and  $\mu > \mu_2$  where one finds  $\Omega_{\text{HF}}^{\text{CDW}} < \Omega_{\text{HF}}^{\text{N}}$ , i.e. a N ground state  $\eta_{\text{N}}$ . However, not all doping values can be realized in this way: according to (31) we can obtain the doping  $\nu$  from the slope of

$$\Omega_{\text{HF}} = \min(\Omega_{\text{HF}}^{\text{CDW}}, \Omega_{\text{HF}}^{\text{N}}),$$

but this is not continuous at  $\mu = \mu_j$ ,  $j = 1, 2$ , where the CDW state changes to the N state. The mean field phases can be determined by the following four doping values,

$$\nu_{X,j} \stackrel{\text{def}}{=} - \left. \frac{\partial(\Omega_{\text{HF}}^X/L^2)}{\partial\mu} \right|_{\mu=\mu_j}, \quad j = 1, 2, \quad X = \text{CDW, N} \quad (35)$$

as follows. The system is in the CDW phase in the doping regime  $\nu_{\text{CDW},1} \leq \nu \leq \nu_{\text{CDW},2}$  and in the N phase for  $\nu \leq \nu_{\text{N},1}$  and  $\nu \geq \nu_{\text{N},2}$ . However, in the regions  $\nu_{\text{N},1} < \nu < \nu_{\text{CDW},1}$  and  $\nu_{\text{CDW},2} < \nu < \nu_{\text{N},2}$  the mixed state in (33), with  $\lambda$  determined by (34), has lower energy than either of the pure Slater states. We refer to the latter as a *mixed phase*. We emphasize that mixed phases occur in large parts of the phase diagram; e.g. for  $t = 1$ ,  $t' = 0$  and  $V = 4$  we find  $\nu_{\text{CDW},1} = \nu_{\text{CDW},2} = 0.5$  and  $\nu_{\text{N},1} = 1 - \nu_{\text{N},2} = 0.30(1)$ .

The results described above have the following physical interpretation (we only discuss the regions close to  $\mu = \mu_2$  since the other one is similar). In the CDW phase one has the effective band relations (see Appendix C.1)

$$e_{\pm}(\mathbf{k}) = -4t' \cos(k_1) \cos(k_2) + q_0 - \mu \pm \sqrt{(-2t + q_1)^2 [\cos(k_1) + \cos(k_2)]^2 + \Delta^2}. \quad (36)$$

This shows that the CDW phase has a band gap  $2|\Delta|$ , and as long as  $\mu$  is in this gap, changing it cannot affect doping. Thus the HF energy is a linear function of  $\mu$  with slope  $\nu_{\text{CDW}} = 0.5$  (half-filling) in this region. The N phase is not gapped and doping can be monotonically increased by increasing  $\mu$ , and therefore the HF energy is a strictly concave function of  $\mu$ . Thus, as we try to increase doping by increasing  $\mu$  in the CDW phase, the HF energy of the N phase decreases faster than the HF energy of the CDW phase, and when both energies become equal at  $\mu = \mu_2$  the doping  $\nu_{\text{N},2}$  in the N phase is significantly larger than the doping  $\nu_{\text{CDW},2}$  in the CDW phase.

A possible interpretation of the mixed state in (33) is a phase-separated state in which parts of the system are in the CDW phase and parts in the N phase [7, 12]. We can therefore conclude that, for  $\nu_{\text{N},2} < \nu < \nu_{\text{CDW},2}$ , a phase-separated state has lower variational energy than any simple mean field state. However, we emphasize that the occurrence of a mixed phase does not necessarily imply phase separation, but it nevertheless proves that a true HF ground state is very different from any state that can be described by a simple mean field ansatz (32) (a true HF ground state can in principle be found by unrestricted HF theory). Thus mean field theory allows to determine those regions in phase space where non-conventional physics (not describable by mean field theory) is to be expected.

---

<sup>5</sup>The accuracy of  $\mu_2$  reached in our computations is actually greater than what the numerical error given here suggests. A similar remark applies to other numerical results given in this paper.

It is interesting to note that, for non-zero  $t'$ , it is possible to have a CDW phase also away from half-filling. This can be seen by computing a plot similar to Figure 3 but with  $t' = -0.2$ , for example. One still finds that the CDW energy  $\Omega_{\text{HF}}^{\text{CDW}}$  as a function of  $\mu$  is a straight line in most of the interval  $\mu_1 < \mu < \mu_2$ , but as  $\mu$  approaches  $\mu_2$  from the left, this curve starts to bend so that  $\nu_{\text{CDW},2} = 0.53(1) > 0.5$ . There is no bending of  $\Omega_{\text{HF}}^{\text{CDW}}$  close to  $\mu = \mu_1$ , however, and  $\nu_{\text{CDW},1} = 0.5$ . Thus at  $t = 0$ ,  $t' = -0.2$ ,  $V = 4$  it is possible to dope the CDW state on the particle side (i.e. for  $\nu > 0.5$ ) but not on the hole side ( $\nu < 0.5$ ). This shows that the parameter  $t'$  affects the mean field phase diagrams both quantitatively and qualitatively.

Our results for the 2D  $t$ - $t'$ - $V$  model were obtained with MATLAB using the system size  $L = 100$  (i.e.  $100^2$  lattice sites). We checked that this is large enough so that finite size effects are essentially negligible. However, we note that some phase boundaries are slightly affected by finite size effects even at this system size, as discussed in more detail below.

### 3.2 2D Luttinger model

We use HF theory as explained for the 2D  $t$ - $t'$ - $V$  model in the previous section. The reference Hamiltonian can now be written as (using a convenient matrix notation)

$$H_{\text{HF}} = \sum_{\mathbf{k} \in \Lambda_a^*} (c_+^\dagger(\mathbf{k}), c_-^\dagger(\mathbf{k})) \begin{pmatrix} \varepsilon_+(\mathbf{k}) + q_0 + q_1 - \mu_a & \Delta \\ \Delta & \varepsilon_-(\mathbf{k}) + q_0 - q_1 - \mu_a \end{pmatrix} \begin{pmatrix} c_+(\mathbf{k}) \\ c_-(\mathbf{k}) \end{pmatrix} \quad (37)$$

with variational parameters  $q_0$ ,  $q_1$  and  $\Delta$ .

The grand canonical potential corresponding to this reference Hamiltonian, evaluated for the Hamiltonian in (13), is denoted by  $\Omega_a$ ; see Appendix C.2.3 for explicit formulas. It is important to note that this is only the antinodal contribution and that the total grand canonical potential of the 2D Luttinger model is

$$\Omega = \Omega_a + \mathcal{E}_a \quad (38)$$

with the energy constant  $\mathcal{E}_a$  in (22)–(26) taking into account the contributions from the other fermion flavors ( $r, s$ ),  $r = \pm$  and  $s = \pm, 2$ . Note that  $\Omega_a$  is a function of  $\mu_a$  (rather than  $\mu$ ), and that the filling constraint following from our general discussion of HF theory in Appendix B is

$$\nu_a = -\frac{1}{(\kappa L)^2} \frac{\partial \Omega_a}{\partial \mu_a}. \quad (39)$$

On the other hand, the filling constraint in (31) should still hold true but with  $\Omega_{\text{HF}}$  replaced by  $\Omega$  in (38). This implies the following consistency condition

$$\frac{\partial(\mathcal{E}_a/L^2)}{\partial \mu} = -\nu + \kappa^2 \nu_a \frac{\partial \mu_a}{\partial \mu} \quad (40)$$

which must be fulfilled for the parameters  $\mu_a$  and  $\mathcal{E}_a$  given in Section 2.2. This identity is non-trivial and provides an important check of our computations. We therefore include details of its verification in Appendix C.3.

The calculation of the grand canonical potential of the antinodal CDW phase is done as follows (the normal phase is treated identically). For fixed  $\mu$ , we make an ansatz for the antinodal filling  $\nu_a$ . Solving (19) for  $Q_0$  then gives us  $\mu_a$  using (16). We proceed by minimizing the grand canonical potential (38) with respect to the variational parameters  $q_0$ ,  $q_1$  and  $\Delta$ . This in turn gives us a specific value for the antinodal filling to be compared with our initial guess. We repeat the above procedure until a self-consistent solution is obtained for  $\nu_a$ . An example of a resulting curve for  $\Omega$  vs.  $\mu$  is given in Figure 4.

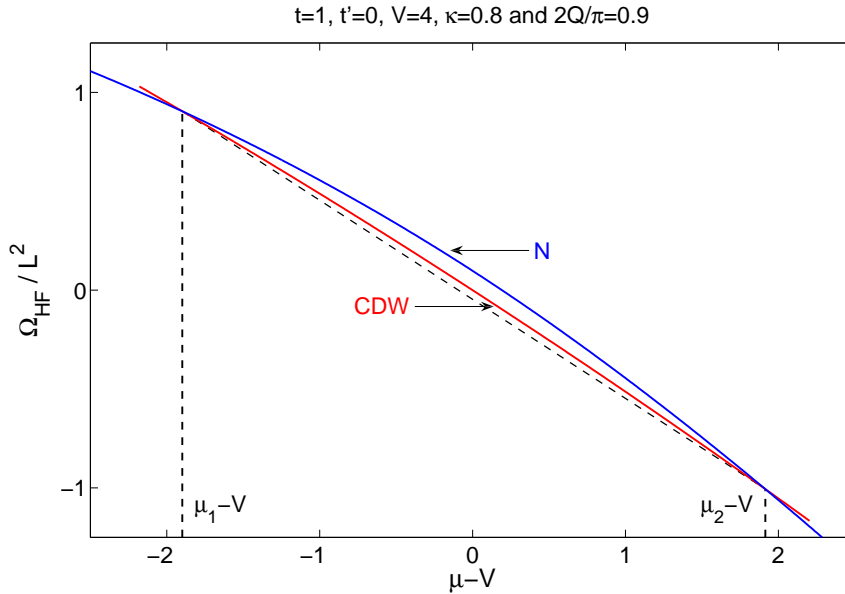


Figure 4: Hartree-Fock energies vs.  $\mu$  as in Figure 3 but now for the 2D Luttinger model at  $\kappa = 0.8$  and  $Q = 0.45\pi$  ( $V = 4$ ,  $t = 1$ ,  $t' = 0$ ). Shown are the energies of the antinodal charge-density-wave (CDW) and normal (N) phases. Again there is an interval  $\mu_1 < \mu < \mu_2$  for which the CDW energy is lower, but unlike Figure 3, this energy now deviates from a straight line (dashed in the figure). This is due to the nodal fermions that change the total filling  $\nu$  even though the antinodal fermions are half-filled and gapped. This kind of plot proves the existence of a partially gapped mean field phase in the 2D Luttinger model.

For the numerical calculation of  $\Omega_a$ , we fix the number of momenta in the antinodal Fourier space regions (10) to 6400. Then  $L = 80\sqrt{2}/\kappa$ , which is large enough so that finite size effects are smaller than the symbol size in our figures. Furthermore, at this system size we can safely replace the Riemann sums in Appendix A.2.3 by integrals.

## 4 Phase diagrams

In this section, we present and discuss mean field phase diagrams for the 2D  $t$ - $t'$ - $V$  model and the 2D Luttinger model.

## 4.1 2D $t$ - $t'$ - $V$ model

Figures 1(a), 5 and 6 give various phase diagrams of the 2D  $t$ - $t'$ - $V$  model. Shown are the phase boundaries of the CDW phase, the N phase, and the mixed phase (indicated by horizontal lines) and how they depend on filling  $\nu$ , coupling  $V$  and nnm hopping  $t'$ .

As seen in Figure 1(a), for  $t' = 0$  the CDW phase is only stable at half-filling  $\nu = 0.5$ , and there is a significant mixed region away from half-filling. The size of this region grows with increasing  $V$ . The invariance of the phase diagram under  $\nu \rightarrow 1 - \nu$  is a consequence of particle-hole symmetry and  $t' = 0$ . We found that all phase boundaries in this figure are insensitive to finite size effects.

The dependence of the phase boundaries on  $t'$  and  $\nu$  for  $V = 4$  is shown in Figure 5. Due to particle-hole symmetry this phase diagram is invariant under  $(t', \nu) \rightarrow (-t', 1 - \nu)$ , and we therefore only discuss  $t' \leq 0$ . For  $0 \leq -t' < 0.15(3)$ , the effect of  $t'$  is small and, in particular, the CDW phase exists only at half-filling. However, for  $0.15(3) < -t' < 0.21(3)$  it is possible to dope the CDW phase on the particle (but not on the hole) side, as discussed in Section 3.1. For even larger values of  $-t'$ , the CDW phase can be doped both on the particle and the hole side, and the mixed region becomes smaller with increasing  $-t'$  and eventually vanishes. Note that the phase boundaries between the N and the mixed phases do not change much with  $-t'$ , for example,  $\nu_{N,1} = 0.70(1)$  and  $0.69(1)$  for  $-t' = 0$  and  $0.3$ , respectively. Moreover, the phase boundary between the CDW and the mixed phases at the hole side for  $-t' > 0.21(3)$  is, to a good approximation, a straight line. The small wiggles of the phase boundary between the CDW and the mixed phases on the particle side for  $-t' > 0.18(3)$  are due to (minor) finite size effects, but all other phase boundaries are quite insensitive; the same is true for the phase diagrams in Figure 6.

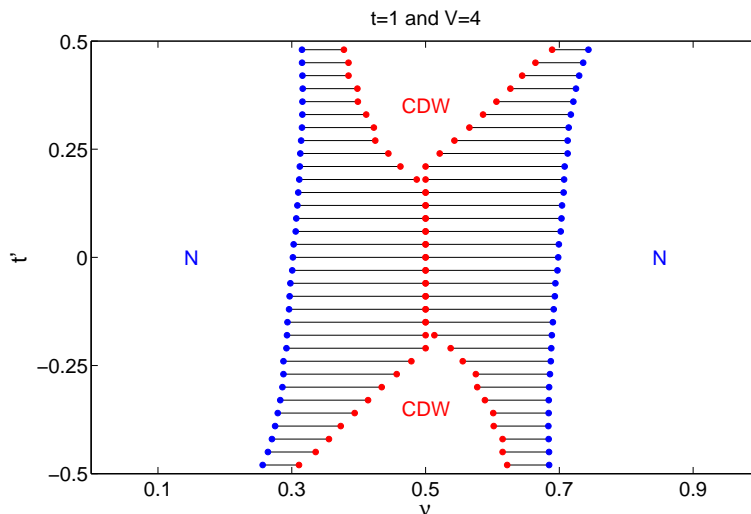


Figure 5: Mean field phase diagram of the 2D  $t$ - $t'$ - $V$  model at zero temperature: next-nearest-neighbor hopping  $t'$  vs. filling  $\nu$  at  $t = 1$  and  $V = 4$ . Shown are the charge-density-wave (CDW), normal (N), and mixed (horizontal lines) phases.

The dependence of the phase boundaries on  $t'$  can also be seen in Figures 6(a) and (b)



showing the  $V$  vs.  $\nu$  phase diagrams for  $t' = -0.2$  and  $-0.4$ , respectively. Note that, for non-zero  $t'$ , there is a critical coupling value  $V_c > 0$  below which no CDW phase exists (e.g.  $V_c = 0.8(1)$  for  $t' = -0.2$ ), and that there is a phase boundary between the CDW and N phases. Moreover, for strong coupling, the CDW phase broadens out and increasingly dominates the phase diagram (only visible in (b)). The phase boundary between the CDW and N phases is quite sensitive to finite size effect, and it is difficult to determine from our numerical data if it is a first- or second order phase transition. Finally, to see how the phase diagram evolves with  $t'$  it is instructive to compare Figures 1(a) with Figures 6(a) and (b).

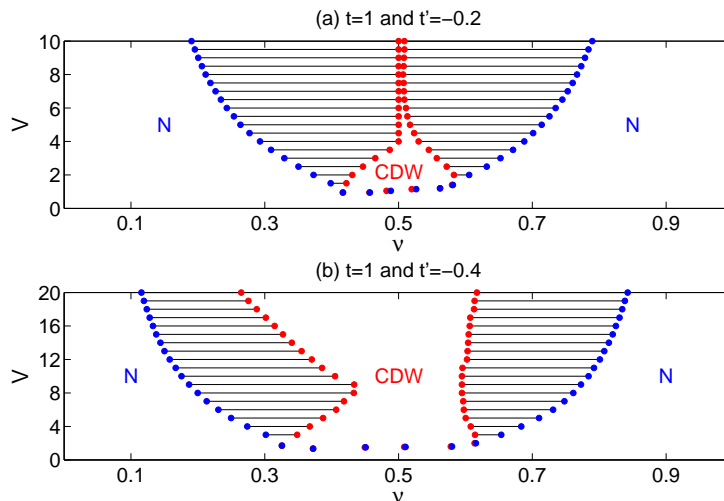


Figure 6: Mean field phase diagrams of the 2D  $t$ - $t'$ - $V$  model at zero temperature: coupling  $V$  vs. filling  $\nu$  at  $t' = -0.2$  in (a) and  $t' = -0.4$  in (b) ( $t = 1$ ). Shown are the charge-density-wave (CDW), normal (N), and mixed (horizontal lines) phases.

## 4.2 2D Luttinger model

Apart from Figure 1(b), all our phase diagrams for the 2D Luttinger model have been computed for  $t = 1$ ,  $V = 4$  and  $t' = 0$  or  $-0.2$ . These parameter choices are partly motivated by our results on the 2D  $t$ - $t'$ - $V$  model. To be specific, for  $t' = -0.2$ , the phase diagram displays several, qualitatively different, features near half-filling, while  $V$  is still of the same order of magnitude as  $t$ ; see Figure 6(a). Furthermore, there is an interesting transition near  $V = 4$  and  $t' = -0.2$  at which it becomes possible to both particle- and hole-dope the CDW phase. Other than this, there is nothing special about these parameter values.

As mentioned in the introduction, a main result of this paper is that the 2D Luttinger model indeed has a phase in which the antinodal fermions are gapped and half filled, as conjectured in [1, 2]. Figure 1(b) shows one example with fixed values of  $Q$  and  $\kappa$  (as

explained later, we can in fact eliminate the parameter  $Q$  in this figure by the requirement  $Q = Q_0$ ). Similar to the 2D  $t$ - $t'$ - $V$  model, we again find a CDW phase, a N phase, and a mixed phase in-between. However, for  $\kappa < 1$ , the mixed phase is typically much smaller than for the 2D  $t$ - $t'$ - $V$  model; cf. Figure 1(a).

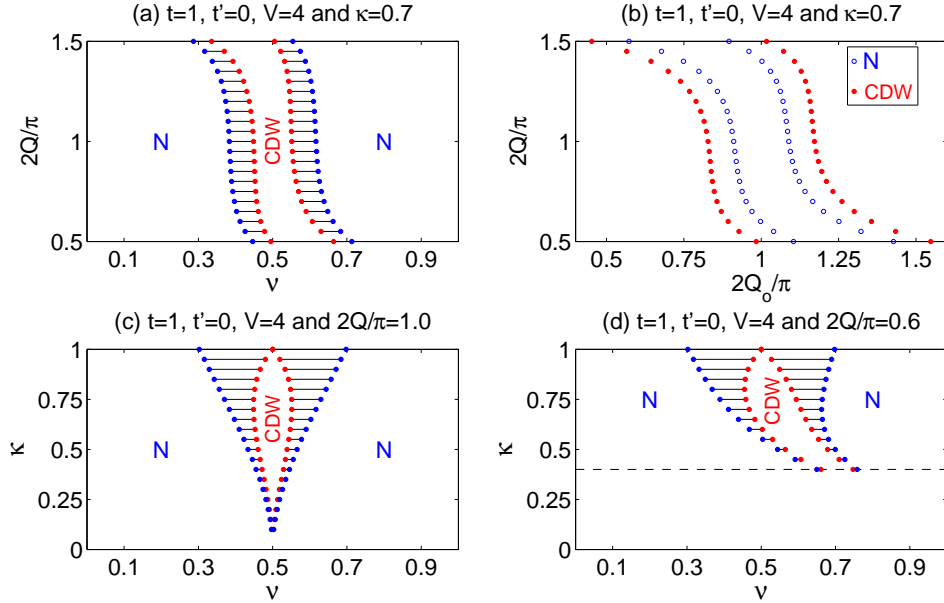


Figure 7: Mean field phase diagrams of the 2D Luttinger model at zero temperature,  $t = 1$ ,  $t' = 0$ ,  $V = 4$ , and for different values of the antinodal region size  $\kappa$  and nodal linearization point  $Q$ . Shown are the charge-density-wave (CDW), normal (N), and mixed (horizontal lines) phase boundaries of the antinodal fermions. (a)  $Q$  vs. total filling  $\nu$  at  $\kappa = 0.7$  (results for other values of  $\kappa$  are similar). (b)  $Q$  vs. nodal Fermi surface location  $Q_0$  at the four phase boundaries in Figure (a). (c)  $\kappa$  vs.  $\nu$  at  $Q = 0.5\pi$ . (d)  $\kappa$  vs.  $\nu$  at  $Q = 0.3\pi$ . Note that we have to restrict to  $\kappa > |1 - \frac{2Q}{\pi}|$  as indicated by the dashed line. Due to particle-hole symmetry, the corresponding result for  $Q = 0.7\pi$  can be obtained as  $\nu \rightarrow 1 - \nu$ .

An important question is how sensitively the results depend on  $Q$  and  $\kappa$ . We find that the qualitative features of the phase diagrams are robust and the quantitative dependence on  $Q$  is weak. However, the quantitative dependence on  $\kappa$  is more pronounced. To be more specific, Figures 7(a)–(d) give representative examples for  $t' = 0$ : (a) shows how the phase boundaries depend on  $Q$  if  $\kappa$  is fixed, while (c) and (d) show how they change with  $\kappa$  for fixed  $Q$ . We note that the almost vertical phase boundaries found in Figure 7(a) for  $Q$  near  $\pi/2$  is not special to the current choice of  $\kappa$  and  $t'$ . Particle-hole symmetry and  $t' = 0$  imply that the phase boundaries are invariant under  $(Q, \nu) \rightarrow (\pi - Q, 1 - \nu)$ . This and  $Q = \pi/2$  explain the symmetry of Figure 7(c). Recall that  $\kappa$  is restricted by (12) to lie in the range  $|1 - \frac{2Q}{\pi}| < \kappa < 1$ .

Figure 7(b) shows  $Q$  as a function of the nodal Fermi surface location, parameterized

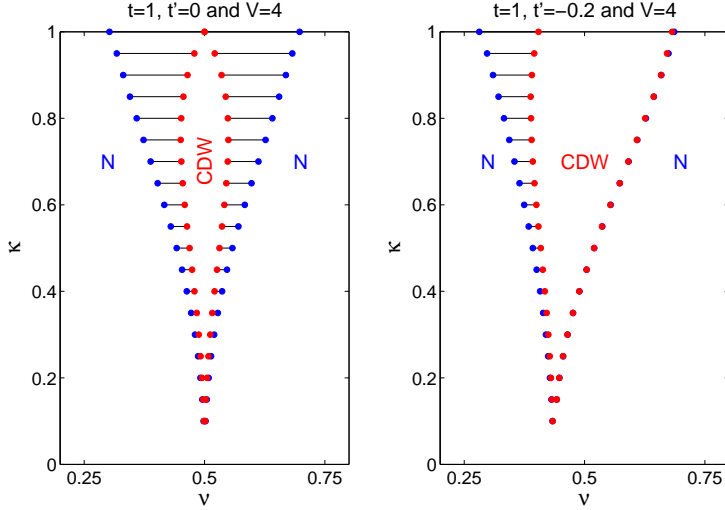


Figure 8: Mean field phase diagrams of the 2D Luttinger model at zero temperature,  $t = 1$ ,  $V = 4$  and  $t' = 0$  (left) respectively  $t' = -0.2$  (right): antinodal region size  $\kappa$  vs. filling  $\nu$ . Shown are the charge-density-wave (CDW), normal (N), and mixed (horizontal lines) phases of the antinodal fermions. The parameter  $Q$  is determined such that the nodal points are located on the nodal Fermi surface arcs at each phase boundary, i.e.  $Q = Q_0$ .

by  $Q_0$ , at the four phase boundaries in 7(a). These figures suggest that one can fix  $Q$  by the requirement  $Q = Q_0$  using the following iterative procedure: given  $Q = Q_n$  one can compute  $Q_0$  by solving the mean field equations and then set  $Q_{n+1} = Q_0$ . We generally find that the sequence  $\{Q_n\}_{n=1,2,\dots}$  converges quickly independent of the starting value for  $Q$ . One can thus eliminate the parameter  $Q$  and obtain phase diagrams depending only on  $\kappa$ .

Figure 8 shows two examples of such phase diagrams, the left for  $t' = 0$  and the right for  $t' = -0.2$ . Comparing the left diagram with Figure 7(c), one finds that the filling values at the four phase boundaries agree up to an error  $\pm 0.002$ . Since  $Q$  varies over an extended interval in Figure 8, while it is fixed at  $\pi/2$  in 7(c), this further demonstrates the insensitivity of the phase boundaries to changes in  $Q$ . The same feature holds true for the right diagram. Moreover, Figure 8 shows again the qualitative changes of the phase diagram induced by non-zero  $t'$ . For  $t' = -0.2$ , the hole side of the phase diagram is similar to the one for  $t' = 0$ , but on the particle side, one no longer finds a mixed region. Instead there is a continuous transition between the CDW and the N phase.

Figure 9 compares the effect of varying the temperature  $1/\beta$  on the phase diagrams of the 2D  $t$ - $t'$ - $V$  model (a) and the 2D Luttinger model for  $\kappa = 0.8$  and  $Q = Q_0$  (b). For the 2D  $t$ - $t'$ - $V$  model at finite temperature, it becomes possible to dope the CDW phase away from half-filling. Moreover, the mixed phase decreases in size as temperature is raised from zero, and it completely disappears at  $1/\beta = 0.50(2)$ . For larger values of  $1/\beta$ , there is a

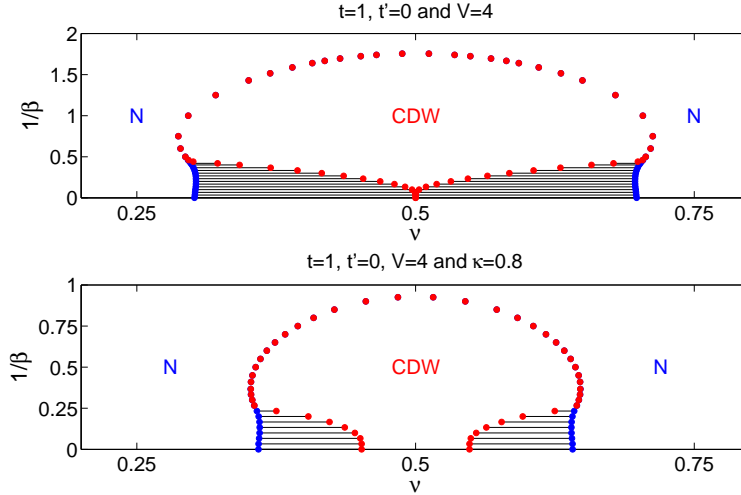


Figure 9: Comparison between the temperature ( $1/\beta$ ) vs. filling ( $\nu$ ) mean field phase diagrams of the 2D  $t$ - $t'$ - $V$  model (a) and the 2D Luttinger model (b) for  $t = 1$ ,  $t' = 0$  and  $V = 4$ . In (b),  $\kappa = 0.8$  and  $Q$  is fixed by the condition  $Q = Q_0$  at the phase boundaries. Shown are the charge-density-wave (CDW), normal (N), and mixed (horizontal lines) phases. Note the different temperature scales in the two plots.

continuous transition between the CDW and N phase. The qualitative features of the 2D Luttinger model at non-zero temperature are quite similar to the 2D  $t$ - $t'$ - $V$  model, except that the CDW phase is only partially gapped and the overall temperature scale is reduced. For example, the mixed phase now disappears at  $1/\beta = 0.25(2)$ . We note that in computing the filling contribution from the nodal fermions, we have assumed for simplicity that there are only bosonic excitations from the ground state, i.e. the total number of nodal fermions is independent of temperature. We leave it to future work to investigate whether or not this is a justified assumption.

Finally, Figure 10 compares phase diagrams of the 2D Luttinger model obtained using the exact antinodal band relation in (27) (open circles) to the ones obtained using the Taylor series approximated ones in (11) (full circles). Note that, for  $t' = 0$  (left), there are only small quantitative differences. For  $t' = -0.2$  (right), however, there are larger deviations, in particular for  $\nu > 0.5$  and  $\kappa > 0.6$ : in the former case we find a mixed region between the CDW- and N phases, but in the latter case this mixed region is absent.

### 4.3 Discussion

In this section, we discuss some general features of the mean field results for the 2D Luttinger- and 2D  $t$ - $t'$ - $V$  models that we observed in our numerical computations. These observations are also based on phase diagrams not included in the present paper.

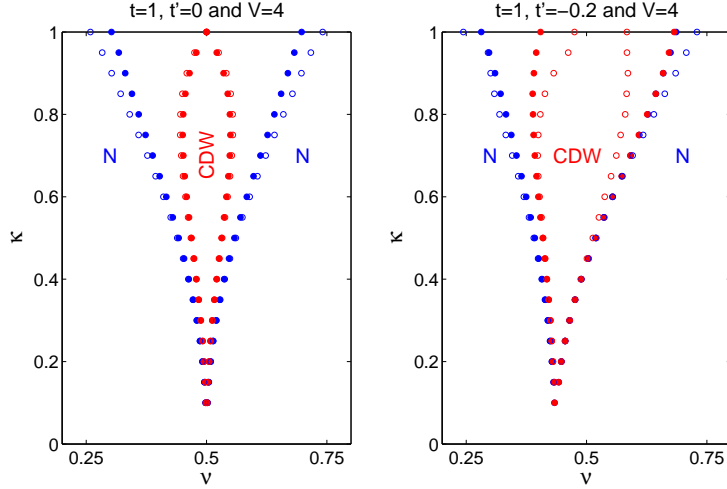


Figure 10: Comparison between the results in Figure 8 obtained with the Taylor series approximated band relations (11) (full circles), and the ones obtained using the full band relations (27) (open circles). Note that the results agree well for  $t' = 0$ , but there are some differences for  $t' = -0.2$  and  $\kappa > 0.6$ .

Whenever the CDW and the N phase share a phase boundary in a diagram (i.e. there is no mixed region in between), the CDW order parameter  $\Delta$  goes continuously to zero at the boundary. Such phase boundaries are more difficult to determine numerically than transitions to a mixed phase.

For  $t' = 0$  we only found a CDW phase in the 2D Luttinger model with  $\nu_a = 0.5$ , i.e. the antinodal fermions are half-filled. However, as for the 2D  $t$ - $t'$ - $V$  model, for non-zero  $t'$  it is possible to have a CDW phase with  $\nu_a \neq 0.5$ . In fact, as a general rule of thumb, if the parameters  $V$  and  $t'$  are such that the CDW phase in the 2D  $t$ - $t'$ - $V$  model can be doped, then the 2D Luttinger model has a partially gapped phase with  $\nu_a \neq 0.5$ . The converse is not always true. We expect that the physical properties of the 2D Luttinger model in a gapped phase with  $\nu_a \neq 0.5$  is qualitatively different to one with  $\nu_a = 0.5$ .

Furthermore, as exemplified in Figure 10, when  $t' = 0$  the phase diagram of the 2D Luttinger model is hardly changed if one replaces the Taylor series approximated band relation in (11) by the exact one in (27). For  $t' \neq 0$  and  $\kappa$  close to 1, the results are more sensitive to this replacement.

We note that it is not obvious that the phase boundaries can be fixed unambiguously by the requirement that  $Q = Q_0$  since the  $Q_0$ -value for which this occurs is, in general, different for the N and the CDW phase. However, we found that using the  $Q_0$ -value from the N and the CDW phase leads to results that are very similar: for  $t' = 0$  the discrepancy is typically smaller than the symbol size in our figures, and this is also true for  $t' = -0.2$ , apart from the case when  $\kappa$  is close to one and the full band relation in (27) is used. In

Figures 8-10 we determined the phase diagrams using  $Q_0$  from the CDW phase. When using the  $Q_0$ -values from the N phase, the CDW phase increases slightly in size, while the N phase decreases slightly in size.

We now discuss how the size and location of the nodal arcs evolve in the left diagram of Figure 8 as  $\kappa$  and  $\nu$  are varied. This serves as a representative example for the general case. Consider first fixed  $\kappa$  and  $\nu \leq 0.5$  ( $\nu \geq 0.5$  is analogous). When the system is in the half-filled and partially gapped CDW phase, one finds  $Q_0 = \pi/2$ .<sup>6</sup> As the nodal fermions are hole doped,  $Q_0$  decreases until eventually the CDW phase becomes unstable at some filling  $\nu < 0.5$ . For even smaller values of  $\nu$ , the system is first in a mixed phase, followed by a N phase. When the system goes from the CDW-mixed phase boundary to the N-mixed boundary, the  $Q_0$  value will first increase towards  $\pi/2$ . As an example, when  $\kappa = 0.8$ ,  $Q_0$  is 0.38(1) on the former boundary and 0.44(1) on the latter. Furthermore, when the size of the nodal arcs is increased (i.e. decreasing the value of  $\kappa$ ), the value of  $Q_0$  on the phase boundaries approaches asymptotically  $\pi/2$ .

Finally, in mean field theory, the antinodal fermions in the 2D Luttinger model behave very much as the fermions in the original 2D  $t$ - $t'$ - $V$  model scaled by a factor  $\kappa^2$ . To give an example, when the antinodal fermions are half-filled ( $\nu_a = 0.5$ ), the size of the CDW gap is, to a good approximation, proportional to  $\kappa^2$ . Likewise, the qualitative features of the temperature vs. filling phase diagrams for the 2D  $t$ - $t'$ - $V$  - and 2D Luttinger model are almost identical if the temperature scale of the latter is reduced by a factor  $\approx \kappa^2$ .

## 5 Final remarks

1. Mean field theory is a variational method and therefore not necessarily restricted to weakly coupled systems. For example, there exist interacting fermion Hamiltonians of the type (1) for which mean field theory is exact (examples include Hartree- and BCS-like models; see e.g. [18] for details). Moreover, for many models describing electrons in conventional 3D metals, it is known that mean-field type approximations can give accurate results despite of the presence of strong Coulomb interactions. Nevertheless, for lattice fermion systems of Hubbard-type, standard mean field theory fails in a large part of the parameter regime [7]. In this paper, we demonstrated that it is possible to circumvent this problem by treating parts of the fermion degrees of freedom exactly using bosonization, as proposed in [1, 2]. It is straightforward to extend this approach to the 2D Hubbard model [19].

2. The results in [2] and the present paper suggest that the 2D  $t$ - $t'$ - $V$  model has a qualitatively different behavior in different filling regimes that can be described by different effective Hamiltonians. For example, at half filling there is, on the mean field level, a fully gapped CDW phase that is adequately described by the antinodal Hamiltonian in (13) with  $\kappa = 1$ . Upon doping the system, both the nodal- and the antinodal degrees

---

<sup>6</sup>As noted in Section 2.2 and further discussed in [2], this parameter regime must be interpreted with some care since one has additional back-scattering interaction terms not included in the 2D Luttinger model when  $Q_0 = \pi/2$ .

of freedom become relevant, and the low-energy physics is governed by the 2D Luttinger model with  $\kappa < 1$ . For the special case when the antinodal fermions are gapped, it is possible to describe the system by a pure nodal fermion model that can be solved exactly by bosonization [2]. For large filling ( $\nu$  close to one), the low-energy physics is expected to be dominated by the out-fermions with  $r = +$  and  $s = 2$ . In this regime, the appropriate effective model describes non-interacting fermions with a band relation  $\varepsilon_{+,2}(\mathbf{k}) \propto (k_1^2 + k_2^2)$  [2]. Corresponding statements hold for the in-fermions at small filling ( $\nu$  close to zero).

**3.** A main result of this paper is that the 2D Luttinger model indeed has a partially gapped phase with gapless nodal fermions and gapped antinodal fermions. The possibility to obtain such a phase is insensitive to changes of parameter values and model details like the band relation.

**4.** For  $\kappa = 1$  all degrees of freedom in the 2D Luttinger model are treated in mean field theory (there are no nodal fermions then). One should therefore expect that the phase diagram of the 2D Luttinger model for  $\kappa = 1$  should be qualitatively similar to the one of the 2D  $t$ - $t'$ - $V$  model. Our results show that this is indeed the case, but there are some quantitative differences; compare Figures 5 and 8. Most of these differences are explained by the Taylor series approximation of the antinodal bands (11); cf. Figure 10. The remaining discrepancy is due to the approximation of the interaction vertex mentioned at the end of Section 2.2. As discussed there, it is possible to improve on this approximation [2] and derive a refined 2D Luttinger model that gives back the 2D  $t$ - $t'$ - $V$  model when setting  $\kappa = 1$ .

**5.** There exist parameter values such that the renormalized antinodal coupling constant  $g_a$  in (17) is negative: we found, for example,  $g_a < 0$  for  $t = 1$ ,  $t' = -0.2$ ,  $V = 10$ ,  $\kappa = 0.8$ , and  $2Q/\pi = 0.24$ . However, this and all other such cases we found are barely within the domain of validity of our method; recall (12). We therefore restricted our discussion in this paper to  $g_a > 0$ .

**6.** It is worth noting that our results do not violate the Luttinger theorem [20]: the proof of this theorem assumes a standard connected Fermi surface, and it therefore requires modifications if there is a (partial) gap.

**7.** In this paper, we only presented mean field results for the simplest consistent charge-density-wave ansatz (i.e. only  $q_0$ ,  $q_1$  and  $m_0$  non-zero, see Appendix C). Another interesting possibility is the so-called d-wave charge-density-wave (DDW) phase that has been suggested in the context of high-temperature superconductors [22]. It corresponds to an ansatz with  $q_0$ ,  $q_1$  and  $m_2$  non-zero (this is a special case of the general ansatz in (73)). One can find mean field solutions for which  $m_2 \neq 0$  gives lower energy than  $m_2 = 0$ . However, we never obtained a DDW solution that has lower energy than the CDW solution discussed in the main text. The same result hold for the other mean field order parameters given in Appendix C.

*Note added:* Recently, numerical simulations of the 2D  $t$ - $t'$ - $V$  model using fermionic PEPS [21] produced a phase diagram that is remarkably similar to our Figure 1(a); cf. Figure 22 in [21].

## Acknowledgments

This work was supported by the Göran Gustafsson Foundation and the Swedish Research Council.

## A Model details

The results in the present paper are a slight generalization of the ones derived in [2]. In this appendix we explain how these generalizations are obtained. We also point out the (minor) differences in notation as compared to [2]. In the following, we write “(I.33)” short for “Equation (33) in [2]” etc.

In [2], the lattice constant  $a$  was an important parameter when taking the partial continuum limit in the nodal region. However, in the present paper we can without loss of generality set it to 1. The relation between the fermion operators used here and the ones in [2] is as follows,

$$c(\mathbf{k}) = \frac{2\pi}{L}\hat{\psi}(\mathbf{k}), \quad c_{\pm}(\mathbf{k}) = \frac{2\pi}{L}\hat{\psi}_{\pm,0}(\mathbf{k}). \quad (41)$$

### A.1 2D $t$ - $t'$ - $V$ model

The Hamiltonian in (3) is obtained from the one in (I.19) and (I.25)–(I.28) by inserting  $\hat{u}(\mathbf{p}) = Vu(\mathbf{p})/(8\pi^2)$  and (41), and using

$$\sum_{\mathbf{k}_j \in \text{BZ}} v_{\mathbf{k}_1, \mathbf{k}_2, \mathbf{k}_3, \mathbf{k}_4} c^{\dagger}(\mathbf{k}_1) c(\mathbf{k}_2) c^{\dagger}(\mathbf{k}_3) c(\mathbf{k}_4) = \sum_{\mathbf{k}_j \in \text{BZ}} v_{\mathbf{k}_1, \mathbf{k}_2, \mathbf{k}_3, \mathbf{k}_4} c^{\dagger}(\mathbf{k}_1) c^{\dagger}(\mathbf{k}_3) c(\mathbf{k}_4) c(\mathbf{k}_2),$$

i.e. normal-ordering of the interaction with respect to the trivial vacuum does not generate any additional terms.

We recall that the 2D  $t$ - $t'$ - $V$  model is invariant under the following transformation of parameters:

$$(t, t', V, \mu, \nu) \rightarrow (t, -t', V, 2V - \mu, 1 - \nu). \quad (42)$$

To see this, we make the particle-hole transformation

$$c(\mathbf{k}) \rightarrow c^{\dagger}(-\mathbf{k} + \mathbf{Q}), \quad c^{\dagger}(\mathbf{k}) \rightarrow c(-\mathbf{k} + \mathbf{Q}), \quad t' \rightarrow -t', \quad \mu \rightarrow 2V - \mu$$

in (3) and (8) and find

$$N \rightarrow L^2 - N, \quad H \rightarrow H + (V - \mu)L^2. \quad (43)$$

### A.2 Effective antinodal Hamiltonian

The 2D  $t$ - $t'$ - $V$  Hamiltonian (3) and the effective antinodal Hamiltonian (13) are related through a series of steps which we summarize schematically as

$$H_{tt'V} \approx H_n + H_a + H_{na} + \mathcal{E}_0 \rightarrow H_{\text{eff}} + \mathcal{E}_n + \mathcal{E}_0 = \tilde{H}_a + \mathcal{E}_a. \quad (44)$$



The approximate equality in (44) is the derivation of the 2D Luttinger model from the 2D  $t$ - $t'$ - $V$  model; see Section 5 in [2]. An important feature in this derivation is normal-ordering with respect to a non-trivial reference state  $|\text{vac}\rangle$ . This leads to both constant shifts  $\mu \rightarrow \mu_{r,s}$  of the chemical potentials for the different fermion flavors  $r = \pm$ ,  $s = 0, \pm, 2$ , and to an additive energy constant  $\mathcal{E}_0$ . The arrow in (44) involves integrating out the bosonized nodal fermions in the partition function for the 2D Luttinger model. This gives an additional energy constant  $\mathcal{E}_n$  and, after a local-time approximation [2], an effective Hamiltonian  $H_{\text{eff}}$  for (normal-ordered) antinodal fermions. The normal-ordering is undone on the right-hand side of the equality in (44), leading to the antinodal Hamiltonian (13) and the energy constant (22).

The above-mentioned constants play an important role in the present paper, and we therefore give the details of how to derive them here. Note that  $\varepsilon_{r,0}(\mathbf{k})$  in (I.47) and (I.6) is identical with  $\varepsilon_r(\mathbf{k})$  in (11) (recall that  $k_{\pm} = (k_1 \pm k_2)/\sqrt{2}$ ). Moreover,  $\Lambda_0^*$  in (I.30) and (10) are the same.

### A.2.1 2D Luttinger model

In Section 5.3 in [2], the chemical potential  $\mu$  was fixed by the condition that the one-particle states in the nodal regions  $s = \pm$  were completely filled up to the points  $\mathbf{Q}_{r,\pm} = (rQ, \pm rQ)$ . In the present paper the chemical potential is treated as a free parameter, and the nodal fermions are thus filled up to some points  $(rQ_0, \pm rQ_0)$ , with  $Q_0$  determined by  $\mu$ ; see (49) below. With this generalization, Equations (I.59), (I.60), and (I.9) are modified by the replacement  $Q \rightarrow Q_0$ .

Inserting (I.53), (I.54), and (the modified) (I.59) in (I.63), we obtain for the effective chemical potentials for the different fermion flavors

$$\begin{aligned}\mu_{\pm,0} &= \mu - 2V\nu - 4t' \\ \mu_{\pm,2} &= \mu - 2V\nu + 4t' \mp [4t + 2VC] \\ \mu_{r,\pm} &= \mu - 2V\nu + 4t \cos(Q) + 4t' \cos^2(Q) + 2VC \cos(Q)\end{aligned}\tag{45}$$

with  $C$  in (21) and  $\nu$  in (15).

As argued in Section 5.3 in [2], the 2D  $t$ - $t'$ - $V$  Hamiltonian can be approximated by the normal-ordered 2D Luttinger Hamiltonian without changing the low-energy physics:  $H_{tt'V} \approx H_n + H_a + H_{na} + \mathcal{E}_0$ ; see (I.62). The energy constant appearing here is

$$\mathcal{E}_0 = \sum_{r=\pm} \sum_{s=0,\pm,2} \mathcal{E}_{r,s} + \mathcal{E}_{int}\tag{46}$$

with

$$\mathcal{E}_{r,s} = \sum_{\mathbf{k} \in \Lambda_{r,s}^*} \left(\frac{2\pi}{L}\right)^2 [\epsilon(\mathbf{Q}_{r,s}) + \varepsilon_{r,s}(\mathbf{k})] \langle \text{vac} | \hat{\psi}_{r,s}^\dagger(\mathbf{k}) \hat{\psi}_{r,s}(\mathbf{k}) | \text{vac} \rangle\tag{47}$$

and  $\mathcal{E}_{int}$  in (I.65). The sets  $\Lambda_{r,s}^*$  are the regions of the Brillouin zone corresponding to the  $(r, s)$ -fermions, and they are defined in (I.42). Note that  $\epsilon(\mathbf{Q}_{r,s}) + \varepsilon_{r,s}(\mathbf{k}) \approx \epsilon(\mathbf{Q}_{r,s} + \mathbf{k})$  are the effective band relations of the  $(r, s)$ -fermions; see (I.46), (I.47) and (I.6). The constants

$\mathcal{E}_{r,s}$  thus correspond to the expectation values of the kinetic energy of the  $(r,s)$ -fermions in the reference state  $|\text{vac}\rangle$ . The constant  $\mathcal{E}_{int}$  arises when the interaction and the term proportional to  $-\mu$  are normal-ordered.

### A.2.2 Effective antinodal model

As shown in [2] Section 6.3, integrating out the nodal fermions amounts to replacing the 2D Luttinger model by the normal-ordered effective antinodal Hamiltonian:  $H_n + H_a + H_{na} \rightarrow H_{\text{eff}} + \mathcal{E}_n$ . The additional constant is (in the zero temperature limit) the ground state energy of the nodal Hamiltonian,  $\mathcal{E}_n = \langle H_n \rangle$ . It can be computed explicitly [2], but in the present paper we only need its  $\mu$ -derivative given in (26).

In the present paper we work with  $\tilde{H}_a$  in (13) without normal-ordering. To find the precise relation between the Hamiltonians  $H_{\text{eff}}$  and  $\tilde{H}_a$ , we use (I.37), (I.8) and (I.47) to write (I.91) as

$$H_{\text{eff}} = \sum_{\mathbf{k}} \left(\frac{2\pi}{L}\right)^2 \sum_r [\varepsilon_{r,0}(\mathbf{k}) - \mu_0] : \hat{\psi}_{r,0}(\mathbf{k}) \hat{\psi}_{r,0}^\dagger(\mathbf{k}) : + \\ + 2(2V - g_{\text{eff}}) \sum_{\mathbf{p}} \left(\frac{1}{L}\right)^2 \hat{J}_{+,0}(\mathbf{p}) \hat{J}_{-,0}(-\mathbf{p}). \quad (48)$$

Inserting  $\hat{J}_{\pm,0}(\mathbf{p}) = \hat{\rho}_{\pm,0}(\mathbf{p}) - \delta_{\mathbf{p},0} L^2 \nu_{\pm,0}$ , (I.46), (I.50), (41) and (I.59), we obtain  $H_{\text{eff}} = \tilde{H}_a - \mathcal{E}_{-,0} - \mathcal{E}_{+,0} + \mathcal{E}_u$  with  $\tilde{H}_a$  in (13) and the parameters  $g_a$  in (17),  $\mu_a = \mu_0 + g_a \nu_a \kappa^2$ ,  $\mathcal{E}_{\pm,0}$  in (47), and  $\mathcal{E}_u$  in (24). Inserting (45) gives (16).

To compute  $Q_0$  we consider the nodal fermion branch  $r = s = +$  with the band relation  $\varepsilon_{+,+}(\mathbf{k})$  given in (I.47) and (I.6). The condition that these fermions are filled up to  $(Q_0, Q_0)$  is equivalent to  $\varepsilon_{+,+}(\mathbf{k}) - \mu_{+,+} = 0$  for  $\mathbf{k} + (Q, Q) = (Q_0, Q_0)$ , i.e.

$$\sqrt{2}v_F(Q_0 - Q) - \mu_{+,+} = 0 \quad (49)$$

with  $v_F$  in (I.6). From this we can compute  $\mu$  in (19), and inserting (19) in (45) we obtain  $(\mu_0 \stackrel{\text{def}}{=} \mu_{\pm,0})$

$$\mu_0 = \sqrt{2}v_F(Q_0 - Q) - 4t \cos(Q) - 4t'[1 + \cos^2(Q)] - 2VC \cos(Q) \quad (50)$$

which generalizes (I.7).

### A.2.3 Antinodal energy constant $\mathcal{E}_a$

As discussed above, the two Hamiltonians studied in this paper are related as  $H_{tt'V} \rightarrow \tilde{H}_a + \mathcal{E}_a$  with the total energy constant  $\mathcal{E}_a \stackrel{\text{def}}{=} \mathcal{E}_n + \mathcal{E}_0 - \mathcal{E}_{+,2} - \mathcal{E}_{-,2} + \mathcal{E}_u$ . Inserting (46) and using (45) we can write this as in (22) with

$$\mathcal{E}_{kin} = \mathcal{E}_{+,2} + \mathcal{E}_{-,2} + 4\mathcal{E}_{+,+} \quad (51)$$

where we use  $\mathcal{E}_{+,+} + \mathcal{E}_{+,-} + \mathcal{E}_{-,+} + \mathcal{E}_{-,-} = 4\mathcal{E}_{+,+}$  due to symmetry. Note that  $\mathcal{E}_{\pm,0}$  in (46) drops out due to undoing the normal-ordering of the antinodal fermions.

In the limit of large  $L$ , we can compute  $\mathcal{E}_{r,s}/L^2$  as Riemann integrals (see (47)),

$$\iint_{S_{r,s}} \frac{d^2k}{(2\pi)^2} [\epsilon(\mathbf{Q}_{r,s}) + \varepsilon_{r,s}(\mathbf{k})], \quad (52)$$

with  $S_{r,s} \subseteq \Lambda_{r,s}^*$  the set of all occupied states  $\mathbf{k}$  in  $|\text{vac}\rangle$ . The  $(+, 2)$ -fermions are completely empty, and thus  $\mathcal{E}_{+,2} = 0$ . The  $(-, 2)$ -fermions are completely filled, i.e.  $S_{-,2} = \Lambda_{-,2}^*$ . Using (I.42), (I.47) and (I.6) we get

$$\frac{\mathcal{E}_{-,2}}{L^2} = \int_{-(1-\kappa)\pi/\sqrt{2}}^{(1-\kappa)\pi/\sqrt{2}} \frac{dk_+}{2\pi} \int_{-(1-\kappa)\pi/\sqrt{2}}^{(1-\kappa)\pi/\sqrt{2}} \frac{dk_-}{2\pi} [-4(t+t') + (t+2t')(k_+^2 + k_-^2)]. \quad (53)$$

The  $(+, +)$ -fermions are filled up to  $\mathbf{k} + (Q, Q) = (Q_0, Q_0)$ , i.e.  $S_{+,+}$  contains all  $\mathbf{k} \in \Lambda_{+,+}^*$  with  $k_+ \leq \sqrt{2}(Q_0 - Q)$ . We thus obtain from (I.42) and (I.47)

$$\frac{\mathcal{E}_{+,+}}{L^2} = \int_{-(\kappa\pi+2Q-\pi)/\sqrt{2}}^{\sqrt{2}(Q_0-Q)} \frac{dk_+}{2\pi} \int_{-(1-\kappa)\pi/\sqrt{2}}^{(1-\kappa)\pi/\sqrt{2}} \frac{dk_-}{2\pi} [-4t \cos(Q) - 4t' \cos^2(Q) + v_F k_+] \quad (54)$$

with  $v_F$  in (I.6). Computing these integrals we obtain the result in (23). Finally, for  $\mathcal{E}_{int}$  we insert (I.53), (I.54) and (I.59) in (I.65) and obtain by straightforward but somewhat lengthy computations (25).

## B Hartree-Fock theory: Generalities

For the convenience of the reader, we collect here the main facts about Hartree-Fock theory at non-zero temperature. A more detailed account can be found in [4, 23].

### B.1 Thermal equilibrium states

Many interacting fermion models, including the ones discussed in the present paper, are given by a Hamiltonian as defined in (1). The restriction to a finite number  $\mathcal{N}$  of one-particle quantum numbers amounts to having both short- and long distance cutoffs in the model.

The thermal equilibrium state of (1) at inverse temperature  $\beta$  is obtained as the minimum over all density matrices  $\rho$  of the grand canonical potential

$$\Omega(\rho) \stackrel{\text{def}}{=} \text{Tr}(\rho H) - \frac{1}{\beta} S(\rho) \quad (55)$$

under the particle number constraint

$$\langle N \rangle = -\frac{\partial \Omega}{\partial \mu} = N_0 \quad (56)$$

with “Tr” the trace in the fermion Fock space,  $N_0$  some given non-negative integer and

$$S(\rho) \stackrel{\text{def}}{=} -\text{Tr}(\rho \ln(\rho)) \quad (57)$$

the entropy of the state. The (unique) global minimum of  $\Omega(\rho)$  is obtained for the *Gibbs* state

$$\rho_{\text{Gibbs}} = \frac{e^{-\beta H}}{\text{Tr}(e^{-\beta H})}. \quad (58)$$

## B.2 Unrestricted Hartree-Fock theory

HF theory at non-zero temperature amounts to restricting the search for the minimum of  $\Omega(\rho)$  to the set of all *HF Gibbs* states defined as follows,<sup>7</sup>

$$\rho_{\text{HF}} = \frac{e^{-\beta H_{\text{HF}}}}{\text{Tr}(e^{-\beta H_{\text{HF}}})} \quad (59)$$

with

$$H_{\text{HF}} = \sum_{kl} h_{kl} c_k^\dagger c_l \quad (60)$$

a Hamiltonian for non-interacting fermions and  $h_{kl}$  the matrix elements of a self-adjoint  $\mathcal{N} \times \mathcal{N}$  matrix  $\mathbf{h}$ . We refer to  $\mathbf{h}$  as variational one-particle Hamiltonian.

Note that we do not consider the most general definition of a HF state; one could also allow for states for which  $U(1)$  gauge invariance is broken (see the remark in B.3), or states that are combinations of a pure state and a HF Gibbs state (see [4] for details).

One can compute the grand canonical potential  $\Omega_{\text{HF}} \stackrel{\text{def}}{=} \Omega(\rho_{\text{HF}})$  for such HF Gibbs states in terms of the eigenvalues  $e_\lambda$  and corresponding orthonormal eigenvectors  $f_\lambda$  of  $\mathbf{h}$  as follows,

$$\begin{aligned} \Omega_{\text{HF}} = & \sum_{kl} (t_{kl} - \mu \delta_{kl}) \gamma_{lk} + \sum_{klmn} v_{klmn} (\gamma_{mk} \gamma_{nl} - \gamma_{ml} \gamma_{nk}) \\ & - \frac{1}{\beta} \sum_{\lambda} \left( \frac{\beta e_\lambda}{e^{\beta e_\lambda} + 1} + \ln(1 + e^{-\beta e_\lambda}) \right) \end{aligned} \quad (61)$$

with

$$\gamma_{jk} \stackrel{\text{def}}{=} \sum_{\lambda} \frac{1}{e^{\beta e_\lambda} + 1} (f_\lambda)_j \overline{(f_\lambda)_k} \quad (62)$$

and where  $(f_\lambda)_j$  are the components of the eigenvector  $f_\lambda$ . Moreover, the particle number constraint is

$$\langle N \rangle = \sum_{\lambda} \frac{1}{e^{\beta e_\lambda} + 1} = N_0. \quad (63)$$

In unrestricted HF theory one does not make any restriction on the variational one-particle Hamiltonian  $\mathbf{h}$ , and thus one has, in principle,  $\mathcal{N}^2$  real variational parameters. However, the number of variational parameters can often be reduced by the following:

---

<sup>7</sup>All summation indices in this section go over  $1, 2, \dots, \mathcal{N}$ .

**Proposition:** *Local extrema of  $\Omega(\rho)$  in the set of HF Gibbs states are acquired for a Hamiltonian*

$$H_{\text{HF}} = \sum_{kl} (t_{kl} - \mu\delta_{kl}) c_k^\dagger c_l + \sum_{klmn} v_{klmn} (c_k^\dagger c_m \langle c_l^\dagger c_n \rangle + \langle c_k^\dagger c_m \rangle c_l^\dagger c_n - c_k^\dagger c_n \langle c_l^\dagger c_m \rangle - \langle c_k^\dagger c_n \rangle c_l^\dagger c_m) \quad (64)$$

with  $\langle c_k^\dagger c_l \rangle = \gamma_{lk}$ , i.e. when  $\langle \cdot \rangle$  is the expectation value in the state  $\rho_{\text{HF}}$  corresponding to (64).

The proof is outlined at the end of this section. The corresponding result for zero temperature can be found in [4].

It follows that one can restrict the search of the minimum to variational one-particle Hamiltonians of the form  $h_{kl} = t_{kl} - \mu\delta_{kl} + w_{kl}$ , with

$$w_{kl} = \sum_{mn} (v_{knlm} + v_{nkml} - v_{knml} - v_{nkml}) \gamma_{mn} \quad (65)$$

for some possible  $\gamma_{mn}$  (we will come back to this in Section B.3 below). For the models of interest to us, this fact allows to reduce the variational parameters in HF theory considerably. For example, for the 2D  $t$ - $t'$ - $V$  model on a square lattice with  $L^2$  sites one would naively expect  $L^4$  variational parameters in unrestricted HF theory, but using (65) this number can be reduced to  $5L^2$ .

Note that (64) together with  $\langle c_k^\dagger c_l \rangle = \gamma_{lk}$  gives a self-consistent system of equations that is often used in practical implementations of HF theory. However, when restricting HF theory it is important to check that a self-consistent solution found in this way is indeed an absolute minimum of (61) in the set of considered states. Moreover, in restricted HF theory it is important to work with the grand canonical ensemble (i.e. fix  $\mu$  and not the fermion number) even at zero temperature, as explained in the main text.

The  $\gamma_{jk}$  are the components of a self-adjoint matrix  $\boldsymbol{\gamma} = (e^{\beta\mathbf{h}} + \mathbf{1})^{-1}$  called a *one-particle density matrix*, and this matrix completely specifies the corresponding Hartree-Fock Gibbs state. Moreover, the results in (63) and the second line in (61) are equivalent to  $\text{tr}(\boldsymbol{\gamma}) = N_0$  and

$$\frac{1}{\beta} S(\rho_{\text{HF}}) = \text{tr}(\mathbf{h}\boldsymbol{\gamma} + (1/\beta) \ln(\mathbf{1} + e^{-\beta\mathbf{h}})) = -\frac{1}{\beta} \text{tr}(\boldsymbol{\gamma} \ln(\boldsymbol{\gamma}) + (\mathbf{1} - \boldsymbol{\gamma}) \ln(\mathbf{1} - \boldsymbol{\gamma})) \quad (66)$$

with “tr” the  $\mathcal{N} \times \mathcal{N}$  matrix trace. Finally, in the zero-temperature limit  $\beta \rightarrow \infty$ , the one-particle density matrix (62) becomes  $\gamma_{jk} = \sum_\lambda \theta(-e_\lambda) (f_\lambda)_j \overline{(f_\lambda)_k}$ ; see also (30).

*Proof of the Proposition:* To find the variation of the grand canonical potential we use (61) and (66), and we regard  $\boldsymbol{\gamma}$  rather than  $\mathbf{h}$  as variational parameter:  $\Omega_{\text{HF}} = \Omega_{\text{HF}}(\boldsymbol{\gamma})$ . We compute the variation  $\delta\Omega \stackrel{\text{def}}{=} \frac{d}{ds} \Omega_{\text{HF}}(\boldsymbol{\gamma} + s\delta\boldsymbol{\gamma})|_{s=0}$  and obtain

$$\delta\Omega_{\text{HF}} = \sum_{kl} (t_{kl} - \mu\delta_{kl} + w_{kl} - h_{kl}) \delta\gamma_{lk} \quad (67)$$

with  $h_{kl}$  the matrix elements of  $\mathbf{h} = -(1/\beta) \ln[\boldsymbol{\gamma}(\mathbf{1} - \boldsymbol{\gamma})^{-1}]$  and  $w_{kl}$  in (65); the first three terms are obvious, and the last is obtained from the variation of the entropy term in (66). This implies the result.  $\square$

## B.3 Restricted Hartree-Fock theory

The Hamiltonian (1) often has a large symmetry group, and assuming that the HF Gibbs state is invariant under (a subgroup of) these symmetries allows to reduce the number of variational parameters even further. For example, the 2D  $t$ - $t'$ - $V$  model is invariant under translations, parity, and (discrete) rotations. If one restricts to HF Gibbs states that are invariant under all these transformations, the number of variational parameters can be reduced to just two; see Section C.1. However, as discussed in the main text, symmetries of the Hamiltonian are often broken, and it is therefore important to also allow for HF states where (some of) the symmetries are broken.

In practice, one assumes that the one-particle density matrix commutes with some suitably chosen subgroup of the original symmetry group. This leads to restrictions on the matrix elements  $\gamma_{kl}$ , and thus, through (65), on the matrix elements of the variational one-particle Hamiltonian  $\mathbf{h}$ . The latter is true since the proposition stated in Appendix B.2 can be generalized to restricted HF-theory (we plan to present details elsewhere).

**Remark:** We note that the Hamiltonian (1) is invariant under the gauge transformation

$$c_k \rightarrow e^{i\alpha} c_k \quad (68)$$

for real parameters  $\alpha$ . There exists a natural extension of HF theory allowing also for states for which this gauge symmetry is broken. This extension is relevant for models with attractive interactions, and its physical interpretation is e.g. superconductivity.<sup>8</sup> However, since the interaction of the 2D  $t$ - $t'$ - $V$  model is purely repulsive, superconducting HF states cannot occur; see [4] for proof. For the effective antinodal model in (13) there do exist parameter regimes where the coupling constant  $g_a$  is negative and thus a superconducting HF state is possible. However, as discussed in Section 5, Remark 5, we found that this parameter regime is very small. We therefore ignore superconducting HF states throughout this paper.

## C Mean field theory

We give here some additional details on our mean field treatments of the 2D  $t$ - $t'$ - $V$  - and 2D Luttinger models.

### C.1 2D $t$ - $t'$ - $V$ model

#### C.1.1 Symmetries

The 2D  $t$ - $t'$ - $V$  Hamiltonian in (3) is invariant under the symmetry group generated by the following transformations

$$\mathcal{T}_j : c(\mathbf{k}) \rightarrow e^{ik_j} c(\mathbf{k}), \quad \mathcal{P} : c(\mathbf{k}) \rightarrow c(-\mathbf{k}), \quad \mathcal{R} : c(\mathbf{k}) = c(k_1, k_2) \rightarrow c(k_2, -k_1) \quad (69)$$

---

<sup>8</sup>There are other physical interpretations in the context of nuclear- and elementary particle physics.

for  $j = 1, 2$ . The transformations  $\mathcal{T}_1$  and  $\mathcal{T}_2$ ,  $\mathcal{P}$  and  $\mathcal{R}$  correspond to translations by the lattice vectors  $\mathbf{e}_1 = (1, 0)$  and  $\mathbf{e}_2 = (0, 1)$ , parity transformation, and rotation by  $\pi/2$ , respectively.

### C.1.2 Restricted Hartree-Fock theory

We consider HF theory restricted to variational states for which the symmetry is broken down to translations by two sites, i.e. the restricted symmetry group is generated by  $(\mathcal{T}_1)^2$  and  $(\mathcal{T}_2)^2$ . In such a state, one has for the one-particle density matrix

$$\gamma(\mathbf{k}', \mathbf{k}) = \langle c^\dagger(\mathbf{k})c(\mathbf{k}') \rangle = \Theta(\mathbf{k}) \delta_{\mathbf{k}, \mathbf{k}'} + \tilde{\Theta}(\mathbf{k}) \delta_{\mathbf{k}, \mathbf{k}'+\mathbf{Q}} \quad (70)$$

with  $\mathbf{Q} = (\pi, \pi)$  and some functions  $\Theta$  and  $\tilde{\Theta}$  satisfying

$$\Theta(\mathbf{k}) = \overline{\Theta(\mathbf{k})} = \Theta(\mathbf{k} + 2\mathbf{Q}), \quad \tilde{\Theta}(\mathbf{k}) = \overline{\tilde{\Theta}(\mathbf{k} + \mathbf{Q})} = \tilde{\Theta}(\mathbf{k} + 2\mathbf{Q}). \quad (71)$$

Using the fact about HF theory stated in (64)ff we can restrict ourselves to HF potentials of the following form,

$$w(\mathbf{k}_1, \mathbf{k}_2) = \frac{2V}{L^2} \sum_{\mathbf{k}_3, \mathbf{k}_4 \in \text{BZ}} (v_{\mathbf{k}_1, \mathbf{k}_2, \mathbf{k}_3, \mathbf{k}_4} + v_{\mathbf{k}_3, \mathbf{k}_4, \mathbf{k}_1, \mathbf{k}_2} - v_{\mathbf{k}_1, \mathbf{k}_4, \mathbf{k}_3, \mathbf{k}_2} - v_{\mathbf{k}_3, \mathbf{k}_2, \mathbf{k}_1, \mathbf{k}_4}) \gamma(\mathbf{k}_4, \mathbf{k}_3).$$

Inserting (70) and (5)–(6), and using  $u(\mathbf{k} - \mathbf{k}') = \frac{1}{2} \sum_{j=1}^4 u_j(\mathbf{k})u_j(\mathbf{k}')$  with

$$u_{1,2} \stackrel{\text{def}}{=} \cos(k_1) \pm \cos(k_2), \quad u_{3,4} \stackrel{\text{def}}{=} \sin(k_1) \pm \sin(k_2) \quad (72)$$

we obtain

$$w(\mathbf{k}, \mathbf{k}') = \left( q_0 + \sum_{j=1}^4 q_j u_j(\mathbf{k}) \right) \delta_{\mathbf{k}, \mathbf{k}'} + \left( m_0 + \sum_{j=1}^4 i m_j u_j(\mathbf{k}) \right) \delta_{\mathbf{k}, \mathbf{k}'+\mathbf{Q}} \quad (73)$$

with

$$q_0 = 2Vn_0, \quad m_0 = -2V\tilde{n}_0, \quad q_j = -\frac{V}{2}n_j, \quad m_j = -\frac{V}{2}\tilde{n}_j \quad (74)$$

and

$$\begin{aligned} n_0 &= \frac{1}{2L^2} \sum_{\mathbf{k}} [\Theta(\mathbf{k}) + \Theta(\mathbf{k} + \mathbf{Q})], & \tilde{n}_0 &= \frac{1}{L^2} \sum_{\mathbf{k}} \text{Re} \tilde{\Theta}(\mathbf{k}) \\ n_j &= \frac{1}{2L^2} \sum_{\mathbf{k}} [\Theta(\mathbf{k}) - \Theta(\mathbf{k} + \mathbf{Q})] u_j(\mathbf{k}), & \tilde{n}_j &= \frac{1}{L^2} \sum_{\mathbf{k}} \text{Im} \tilde{\Theta}(\mathbf{k}) u_j(\mathbf{k}) \end{aligned} \quad (75)$$

for  $j = 1, 2, 3, 4$ , with all sums over BZ; we used (71) and  $u_j(\mathbf{k} + \mathbf{Q}) = -u_j(\mathbf{k})$ .

### C.1.3 Mean field equations

To find  $\Theta$  and  $\tilde{\Theta}$  we use Fourier transformation and write the reference Hamiltonian in (29) and (32) in matrix form as follows,

$$H_{\text{HF}} = \sum_{\mathbf{k} \in \text{BZ}_{1/2}} (c^\dagger(\mathbf{k}), c^\dagger(\mathbf{k} + \mathbf{Q})) \mathbf{h}(\mathbf{k}) \begin{pmatrix} c(\mathbf{k}) \\ c(\mathbf{k} + \mathbf{Q}) \end{pmatrix}$$

with

$$\mathbf{h}(\mathbf{k}) = \begin{pmatrix} a_+(\mathbf{k}) & b(\mathbf{k}) \\ \frac{a_+(\mathbf{k})}{b(\mathbf{k})} & a_-(\mathbf{k}) \end{pmatrix}$$

and

$$a_+(\mathbf{k}) = \epsilon(\mathbf{k}) + q_0 - \mu + \sum_{j=1}^4 q_j u_j(\mathbf{k}), \quad a_-(\mathbf{k}) = a_+(\mathbf{k} + \mathbf{Q}), \quad b(\mathbf{k}) = m_0 + i \sum_{j=1}^4 m_j u_j(\mathbf{k}), \quad (76)$$

where the sum is restricted to half of the Brillouin zone,  $\text{BZ}_{1/2} \stackrel{\text{def}}{=} \{\mathbf{k} \in \text{BZ} : k_1 > 0\}$ . We now can compute  $\gamma(\mathbf{k}) \stackrel{\text{def}}{=} f(\mathbf{h}(\mathbf{k}))$  for  $f(x) = 1/(e^{\beta x} + 1)$  using the following general result,

$$f(\mathbf{h}(\mathbf{k})) = \frac{f(e_+(\mathbf{k})) + f(e_-(\mathbf{k}))}{2} \mathbf{1} + \frac{f(e_+(\mathbf{k})) - f(e_-(\mathbf{k}))}{2W(\mathbf{k})} \begin{pmatrix} a_1(\mathbf{k}) & b(\mathbf{k}) \\ \frac{a_1(\mathbf{k})}{b(\mathbf{k})} & -a_1(\mathbf{k}) \end{pmatrix}$$

with

$$e_\pm(\mathbf{k}) = a_0(\mathbf{k}) \pm W(\mathbf{k}), \quad W(\mathbf{k}) = \sqrt{a_1(\mathbf{k})^2 + |b(\mathbf{k})|^2}, \quad a_{0,1}(\mathbf{k}) = \frac{1}{2}[a_+(\mathbf{k}) \pm a_-(\mathbf{k})]. \quad (77)$$

The  $e_\pm(\mathbf{k})$  are the eigenvalues of the matrix  $\mathbf{h}(\mathbf{k})$  and equal to the effective mean field band relations. From this and

$$\gamma(\mathbf{k}) = \begin{pmatrix} \Theta(\mathbf{k}) & \tilde{\Theta}(\mathbf{k}) \\ \tilde{\Theta}(\mathbf{k}) & \Theta(\mathbf{k} + \mathbf{Q}) \end{pmatrix}$$

we obtain

$$\begin{aligned} \Theta(\mathbf{k}) &= \frac{1}{2} \left( \frac{1}{e^{\beta e_+(\mathbf{k})} + 1} + \frac{1}{e^{\beta e_-(\mathbf{k})} + 1} \right) + \frac{a_1(\mathbf{k})}{2W(\mathbf{k})} \left( \frac{1}{e^{\beta e_+(\mathbf{k})} + 1} - \frac{1}{e^{\beta e_-(\mathbf{k})} + 1} \right) \\ \tilde{\Theta}(\mathbf{k}) &= \frac{b(\mathbf{k})}{2W(\mathbf{k})} \left( \frac{1}{e^{\beta e_+(\mathbf{k})} + 1} - \frac{1}{e^{\beta e_-(\mathbf{k})} + 1} \right). \end{aligned} \quad (78)$$

By straightforward computations we obtain from (61)

$$\frac{\Omega_{\text{HF}}}{L^2} = e_{\text{HF}} - \sum_{j=0}^4 (q_j n_j + m_j \tilde{n}_j) + V \left( n_0^2 - \tilde{n}_0^2 - \frac{1}{4} \sum_{j=1}^4 (n_j^2 + \tilde{n}_j^2) \right) \quad (79)$$

with

$$e_{\text{HF}} = - \sum_{r=\pm} \frac{1}{L^2} \sum_{\mathbf{k}} \frac{1}{\beta} \ln(1 + e^{-\beta e_r(\mathbf{k})}), \quad (80)$$



$n_j$  and  $\tilde{n}_j$  in (75), and  $e_{\pm}(\mathbf{k})$  in (77). Mean field theory amounts to minimizing  $\Omega_{\text{HF}}$  in (79) with respect to the 10 variational parameters  $q_j$  and  $m_j$ ,  $j = 0, 1, 2, 3, 4$ . Note that, by construction, the saddle point equations  $\partial\Omega_{\text{HF}}/\partial q_j = \partial\Omega_{\text{HF}}/\partial m_j = 0$  are identical with the mean field equations in (74)–(78).

We were only able to find absolute minima of the HF grand canonical potential with

$$q_2 = q_3 = q_4 = m_2 = m_3 = m_4 = 0. \quad (81)$$

It is interesting to note that (81) is equivalent to parity- and rotation invariance of the HF state: for HF states invariant under  $\mathcal{P}$  and  $\mathcal{R}$  one has

$$\Theta(\mathbf{k}) = \Theta(-\mathbf{k}) = \Theta(k_2, -k_1)$$

and similarly for  $\tilde{\Theta}$ . This implies that  $n_j$  and  $\tilde{n}_j$  in (75) vanish for  $j = 2, 3, 4$ , and thus  $q_j = m_j$  for  $j = 2, 3, 4$ . Moreover, if this is true, then the HF equations  $q_1 = -Vn_1/2$  and  $m_1 = -V\tilde{n}_1/2$  are in contradiction unless  $m_1 = 0$ . Note that  $m_j = 0$  for  $j = 1, 2, 3, 4$  is equivalent to

$$\overline{\tilde{\Theta}(\mathbf{k})} = \tilde{\Theta}(\mathbf{k}).$$

We therefore restrict our discussion in the main text to the simplified ansatz in (32) with only three variational parameters  $q_0$ ,  $q_1$  and  $m_0 \stackrel{\text{def}}{=} \Delta$ .

#### C.1.4 Numerical details

We solved the mean field equations given above using MATLAB. We found that it is numerically difficult to minimize the grand canonical potential  $\Omega_{\text{HF}}$  directly, but, similarly as for the Hubbard model [4], one can construct an auxiliary extremization problem for a related potential. This latter auxiliary potential has extrema<sup>9</sup> that coincide with those of  $\Omega_{\text{HF}}$  (in general, the minima of  $\Omega_{\text{HF}}$  correspond to saddle-points of the auxiliary potential). Furthermore, the values of these two potentials are equal at corresponding extrema. This auxiliary potential is numerically well-behaved and it therefore allows to reduce the computational time considerably (we plan to present details on this elsewhere).

## C.2 2D Luttinger model

### C.2.1 Symmetries

While the effective Hamiltonian in (13) naturally inherits the following parity- and rotation symmetries from the 2D  $t$ - $t'$ - $V$  model,

$$\mathcal{P} : c_{\pm}(\mathbf{k}) \rightarrow c_{\pm}(-\mathbf{k}), \quad \mathcal{R} : c_{\pm}(\mathbf{k}) = c_{\pm}(k_1, k_2) \rightarrow c_{\mp}(k_2, -k_1), \quad (82)$$

its translation invariance is

$$\mathcal{T}_{\mathbf{x}} : c_{\pm}(\mathbf{k}) \rightarrow e^{i\mathbf{x}\cdot\mathbf{k}} c_{\pm}(\mathbf{k}) \quad (83)$$

---

<sup>9</sup>By “extrema” we mean here points for which all partial derivatives are zero.

for all translation vectors  $\mathbf{x} = (x_1, x_2)$  with components  $x_1, x_2 \in \mathbb{R}$ . This enhancement of translational symmetry is due to the continuum limit taken when deriving the 2D Luttinger model, and it makes it impossible to distinguish between translations by an even and odd number of lattice sites. We thus have the following symmetry transformations of  $H$  in (13),

$$\mathcal{C}_\alpha : c_\pm(\mathbf{k}) \rightarrow e^{\pm i\alpha} c_\pm(\mathbf{k}) \quad (84)$$

with real  $\alpha$ . We use particle physics terminology and refer to  $\mathcal{C}_\alpha$  as chiral transformation.

### C.2.2 Restricted Hartree-Fock theory

It is known that chiral symmetry breaking in a continuum model corresponds to breaking the translation symmetry from one to two sites in the corresponding lattice model; see e.g. [24]. We thus restrict HF theory to all states invariant under all translations  $\mathcal{T}_\mathbf{x}$  but not under chiral gauge transformations  $\mathcal{C}_\alpha$ , i.e. we make the following ansatz for the one-particle density matrix

$$\gamma_{r'r}(\mathbf{k}', \mathbf{k}) = \langle c_r^\dagger(\mathbf{k}) c_{r'}(\mathbf{k}') \rangle = \delta_{\mathbf{k}, \mathbf{k}'} \Theta_{rr'}(\mathbf{k}) \quad (85)$$

for  $r, r' = \pm$  and some functions  $\Theta_{rr'}$  obeying

$$\overline{\Theta_{rr'}(\mathbf{k})} = \Theta_{r'r}(\mathbf{k}). \quad (86)$$

We insert (85) in (65) and obtain

$$H_{\text{HF}} = H_0 + \frac{2g_a}{L^2} \sum_{\mathbf{k}, \mathbf{k}'} \sum_{r, r' = \pm} c_{-r}^\dagger(\mathbf{k}) c_{-r'}(\mathbf{k}') r r' \Theta_{rr'}(\mathbf{k})$$

which is equivalent to (37) with

$$q_0 = g_a n_0, \quad q_1 = -g_a n_1, \quad \Delta = -2g_a \tilde{n}_0 \quad (87)$$

and

$$n_{0,1} = \frac{1}{L^2} \sum_{\mathbf{k}} [\Theta_{++}(\mathbf{k}) \pm \Theta_{--}(\mathbf{k})], \quad \tilde{n}_0 = \frac{1}{L^2} \sum_{\mathbf{k}} \Theta_{+-}(\mathbf{k}) \quad (88)$$

with all  $\mathbf{k}$ -sums over  $\Lambda_a^*$ .

### C.2.3 Mean field equations

The reference Hamiltonian in (37) has exactly the same form as the one treated in Section C.1.3, and we therefore obtain the same results as in (77) and (78) but with

$$a_\pm(\mathbf{k}) = \varepsilon_\pm(\mathbf{k}) + q_0 \pm q_1 - \mu_a, \quad b(\mathbf{k}) = \Delta. \quad (89)$$

Moreover, as in Section C.1.3

$$\frac{\Omega_{\text{HF}}}{L^2} = e_{\text{HF}} - q_0 n_0 - q_1 n_1 - \Delta \overline{\tilde{n}_0} - \overline{\Delta} \tilde{n}_0 + \frac{g_a}{2} (n_0^2 - n_1^2 - 4|\tilde{n}_0|^2) + \mathcal{E}_a \quad (90)$$

with  $e_{\text{HF}}$  as in (80),  $n_{0,1}$  and  $\tilde{n}_1$  in (88) and  $e_\pm(\mathbf{k})$  in (77) and (89).

### C.3 Consistency check

We now show that the condition in (40) holds true. Using (51), (53) and (54) we get

$$\begin{aligned} \frac{\partial(\mathcal{E}_{kin}/L^2)}{\partial\mu} &= [-4t \cos(Q) - 4t' \cos^2(Q) + v_F \sqrt{2}(Q_0 - Q)] \frac{\partial}{\partial\mu} (1 - \kappa) \frac{2Q_0}{\pi} \\ &= [\mu - 2V\nu + 2VC \cos(Q)] \frac{\partial}{\partial\mu} (\nu - \kappa^2 \nu_a) \end{aligned}$$

where we used (49), (45) and (15). Equation (24) implies

$$\frac{\partial(\mathcal{E}_u/L^2)}{\partial\mu} = \nu_a \kappa^2 \left( 1 - 2V \frac{\partial\nu}{\partial\mu} + g_a \kappa^2 \frac{\partial\nu_a}{\partial\mu} \right) + (\mu - 2V\nu) \kappa^2 \frac{\partial\nu_a}{\partial\mu} = \nu_a \kappa^2 \frac{\partial\mu_a}{\partial\mu} + (\mu - 2V\nu) \kappa^2 \frac{\partial\nu_a}{\partial\mu}$$

where we used (16). We use (25) and compute, recalling (21),

$$\frac{\partial\mathcal{E}_{int}}{\partial\mu} = -\nu - (\mu - 2V\nu) \frac{\partial\nu}{\partial\mu} - 2VC \frac{\partial C}{\partial\mu} = -\nu - (\mu - 2V\nu) \frac{\partial\nu}{\partial\mu} - 2VC \cos(Q) \frac{\partial}{\partial\mu} (\nu - \kappa^2 \nu_a).$$

We finally use (26). Recalling (22) and adding the results we find that many terms cancel and that the remaining terms add up to the r.h.s. of (40).

## References

- [1] E. Langmann: A two dimensional analogue of the Luttinger model, [arXiv:math-ph/0606041v3](#) (to appear in Lett. Math. Phys.)
- [2] E. Langmann: A 2D Luttinger model, [arXiv:0903.0055v3\[math-ph\]](#)
- [3] A recent short review is, for example: D. Bonn: Are high-temperature superconductors exotic? *Nature Physics* **2**, 159 (2006)
- [4] V. Bach, E. Lieb, and J. Solovej: Generalized Hartree–Fock theory and the Hubbard model, *J. Stat. Phys.* **76**, 3 (1994)
- [5] J. A. Verges, E. Louis, P. S. Lomdahl, F. Guinea, and A. R. Bishop: Holes and magnetic textures in the two-dimensional Hubbard model, *Phys. Rev. B* **43**, 6099 (1991)
- [6] E. Langmann and M. Wallin: Mean-field approach to antiferromagnetic domains in the doped Hubbard model, *Phys. Rev. B* **55**, 9439 (1997)
- [7] E. Langmann and M. Wallin: Mean field magnetic phase diagrams for the two dimensional  $t - t' - U$  Hubbard model, *J. Stat. Phys.* **127**, 825 (2007)
- [8] D. C. Mattis: Implications of infrared instability in a two-dimensional electron gas, *Phys. Rev. B* **36**, 745 (1987)
- [9] H. J. Schulz: Fermi-surface instabilities of a generalized two-dimensional Hubbard model, *Phys. Rev. B* **39**, 2940 (1989)

- [10] A. Luther: Interacting electrons on a square Fermi surface, Phys. Rev. B **50**, 11446 (1994)
- [11] N. Furukawa, T. M. Rice, and M. Salmhofer: Truncation of a two-dimensional Fermi surface due to quasiparticle gap formation at the saddle points, Phys. Rev. Lett. **81**, 3195 (1998)
- [12] W. R. Czart, S. Robaszkiewicz and B. Tobijaszevska: Charge ordering and phase separations in the spinless fermion model with repulsive intersite interaction, Acta Phys. Pol. A **114**, 129 (2008)
- [13] G. S. Uhrig and R. Vlaming: Inhibition of phase separation and appearance of new phases for interacting spinless fermions, Phys. Rev. Lett. **71**, 271 (1993)
- [14] M. Yu. Kagan, K. I. Kugel, and D. I. Khomskii: Phase separation in systems with charge ordering, J. Exp. & Theor. Phys. **93**, 415 (2001)
- [15] For review and further references see: A. Damascelli, Z. Hussain and Z.-X. Shen: Angle-resolved photoemission studies of the cuprate superconductors, Rev. Mod. Phys. **75**, 473 (2003)
- [16] T. Yoshida *et.al.*: Systematic doping evolution of the underlying Fermi surface of  $\text{La}_{2-x}\text{Sr}_x\text{CuO}_4$ , Phys. Rev. B **74**, 224510 (2006)
- [17] K.M. Shen *et.al.*: Nodal quasiparticles and antinodal charge ordering in  $\text{Ca}_{2-x}\text{Na}_x\text{-CuO}_2\text{Cl}_2$ , Science **307**, 901 (2005)
- [18] E. Langmann: Exactly solvable models for 2D interacting fermions, J. Phys. A: Math. Gen. **37**, 407 (2004)
- [19] J. de Woul and E. Langmann, work in progress
- [20] J. M. Luttinger: Fermi surface and some simple equilibrium properties of a system of interacting fermions, Phys. Rev. **119**, 1153 (1960)
- [21] P. Corboz, R. Orus, B. Bauer and G. Vidal: Simulation of strongly correlated fermions in two spatial dimensions with fermionic Projected Entangled-Pair States, [arXiv:0912.0646v1](https://arxiv.org/abs/0912.0646v1)[cond-mat.str-el]
- [22] S. Chakravarty, R.B. Laughlin, D.K. Morr, and C. Nayak: Hidden order in the cuprates, Phys. Rev. B **63**, 094503 (2001)
- [23] V. Bach and J. Poelchau: Hartree-Fock Gibbs states for the Hubbard model, Markov Proc. and Rel. Fields **2**, 225 (1996)
- [24] E. Langmann and G.W. Semenoff: Strong coupling gauge theory, quantum spin systems and the spontaneous breaking of chiral symmetry, Phys. Lett. B **297**, 175 (1992)